

1 Running head: Genome-scale model for *Anabaena* sp. PCC 7120

2

3 Corresponding author: Patrik R. Jones

4

5 Address: Department of Life Sciences, Imperial College London, Sir Alexander Fleming

6 Building, London, SW7 2AZ, UK

7

8 Phone: +44 (0)20 7594 5213

9

10 E-mail: p.jones@imperial.ac.uk

11

12 Research Area: Biochemistry and Metabolism

13

14 A comprehensively curated genome-scale two-cell model for the heterocystous
15 cyanobacterium *Anabaena* sp. PCC 7120

16

17 David Malatinszky¹, Ralf Steuer², Patrik R. Jones¹

18

19 ¹Department of Life Sciences, Imperial College London, Sir Alexander Fleming Building,
20 London, SW7 2AZ, UK

21 ²Institute for Theoretical Biology, Humboldt University Berlin, 10115 Berlin, Germany

22

23 The genome-scale metabolic model of a nitrogen-fixing filamentous cyanobacterium helps to
24 understand inter- and intra-cellular metabolic interactions and contributes to engineering
25 strategies.

26

27 The research leading to these results has received funding from BBSRC grant
28 (BB/N003608/1) and the People Programme (Marie Curie Actions) of the European Union's
29 Seventh Framework Programme FP7/2007-2013/ under REA grant agreement number
30 317184 (DM). This material reflects only the author's views and the European Union is not
31 liable for any use that may be made of the information contained therein. RS is supported by
32 the "e:Bio –Innovationswettbewerb Systembiologie" [e:Bio – systems biology innovation
33 competition] initiative (CyanoGrowth, FKZ 0316192).

34

35 Corresponding author: Patrik R. Jones (p.jones@imperial.ac.uk)

36

37 Abstract

38

39 *Anabaena* sp. PCC 7120 is a nitrogen-fixing filamentous cyanobacterium. Under nitrogen
40 limiting conditions, a fraction of the vegetative cells in each filament terminally differentiate
41 to non-growing heterocysts. Heterocysts are metabolically and structurally specialized to
42 enable O₂-sensitive nitrogen fixation. The functionality of the filament, as an association of
43 vegetative cells and heterocysts, is postulated to depend on metabolic exchange of electrons,
44 carbon and fixed nitrogen. In the present work, we compile and evaluate a comprehensive
45 curated stoichiometric model of this two-cell system, with the objective function based on the
46 growth of the filament under diazotrophic conditions. The predicted growth rate under
47 nitrogen replete and deplete conditions, as well as the effect of external carbon and nitrogen
48 sources, was thereafter verified. Furthermore, the model was utilized to comprehensively
49 evaluate the optimality of putative metabolic exchange reactions between heterocysts and
50 vegetative cells. The model suggested that optimal growth requires at least four exchange
51 metabolites. Several combinations of exchange metabolites resulted in predicted growth rates
52 that are higher than growth rates achieved by only considering exchange of metabolites
53 previously suggested in the literature. The curated model of the metabolic network of
54 *Anabaena* sp. PCC 7120 enhances our ability to understand the metabolic organization of
55 multi-cellular cyanobacteria and provides a platform for further study and engineering of their
56 metabolism.

57

58 **Introduction**

59 Cyanobacteria are ubiquitous photosynthetic organisms found in almost every habitat on
60 Earth, including hot springs and Antarctic rocks , as well as the fur of some sloths (Aiello,
61 1985). Cyanobacteria are highly diverse in terms of morphology: some species are
62 filamentous, others are unicellular or can form aggregates, several species are capable of
63 nitrogen fixation in differentiated heterocysts, and some form motile hormogonia or spore-
64 like akinetes (Flores and Herrero, 2010; Singh and Montgomery, 2011). In their natural
65 environment, cyanobacteria are often an integral part of complex ecosystems with other
66 species from all three domains of life (Stewart et al., 1983; Adams, 2000; Adams and
67 Duggan, 2008). Several species build up thick microbial mats in extreme environments
68 (Reysenbach et al., 1994), or composite with fungal filaments to form lichens (Rikkinen et al.,
69 2002), while others live inside their symbiotic plant hosts (Adams, 2000). In case of the
70 aquatic *Azolla caroliniana*, a small water fern, a filamentous, heterocyst-forming
71 cyanobacterium is found within the ovoid cavities in the plant's leaves, maintaining a
72 mutually beneficial symbiotic relationship with the plant. This symbiont, *Anabaena azollae*
73 provides fixed nitrogen to the fern and, in return, receives carbon sources and a protected
74 environment from *Azolla* (Hill, 1977; Lechno-Yossef and Nierzwicki-Bauer, 2002). The
75 highly-productive *Azolla-Anabaena* symbiosis has long been recognized as a cheap and
76 effective biofertilizer of tropical rice paddies, and more recently it has been successfully
77 applied in temperate climate as well (Wagner, 1997; Bocchi and Malgioglio, 2010). Outside
78 of its plant host, the free-living form of *Anabaena azollae* has significant contribution to the
79 carbon and nitrogen economy of tropical soils as well, forming microbial communities with
80 other nitrogen-fixing cyanobacteria (Singh, 1950). When living freely, however, *Anabaena*
81 *azollae* only develops 5 to 10% of its cell to heterocysts. This frequency increases up to 25 to
82 30%, when the symbiosis is extended to also include rice. This higher rate of nitrogen-fixation
83 is the result of an adjustment to provide sufficient nitrogen for all three species, i.e. the
84 cyanobacterium, the fern and the co-cultivated rice (de Macale and Vlek, 2004). *Anabaena* sp.
85 PCC 7120 strain, an isolated and sequenced form of *Anabaena azollae*, shows the same
86 developmental pattern of a single heterocyst for every 10 to 20 vegetative cells (Kumar et al.,
87 2010; Ehira, 2013), and acts as a representative model organism of the free-living
88 cyanobacterium. To mimic the productivity of the symbiotic form, *Anabaena* sp. PCC 7120
89 has recently been modified to increase the expression of the HetR protein controlling
90 heterocyst frequency and thus to enhance the organism's potential as a nitrogen biofertilizer.
91 The resulting mutant strain has been reported for its ability to cater rice seedlings with

92 beneficial levels of nitrogen in short-term hydroponic experiments (Chaurasia and Apte,
93 2011). In order to utilize such biochemical traits in designed applied processes, it becomes
94 important to understand community behaviour and metabolic interactions in natural and
95 simple ecosystems where these feature.

96 In fact, *Anabaena* sp. PCC 7120 can alone be argued to form such a very simple yet
97 incompletely understood "community" of cells with multiple metabolic states and
98 interdependent metabolic exchange. Under diazotrophic conditions, approximately every
99 tenth vegetative cell irreversibly transforms into a heterocyst to provide a low-oxygen
100 environment for the nitrogenase enzyme to function (Golden and Yoon, 2003). This enzyme
101 is responsible for the conversion of atmospheric molecular nitrogen into ammonia in a highly
102 energy-expensive reaction, consuming chemical energy stored in 16 molecules of ATP and 8
103 electrons carried by ferredoxin molecules for every molecule of nitrogen assimilated.
104 Furthermore, the nitrogenase is irreversibly inactivated by oxygen which makes oxygenic
105 photosynthesis and nitrogen fixation incompatible processes (Fay, 1992). Therefore, these
106 specialized heterocyst cells undergo a series of changes to minimize the level of internal
107 oxygen, including the deposition of two additional envelope layers around the cell and the
108 degradation of photosystem II and carboxysomes (Wolk et al., 2004; Nicolaisen et al., 2009;
109 Awai et al., 2010). As a result, heterocysts are dependent on vegetative cells as a source of
110 electrons and carbon (Kumar et al., 2010). In return, vegetative cells obtain fixed nitrogen
111 (Meeks and Elhai, 2002). Heterocysts and vegetative cells are therefore mutually
112 interdependent, showing the features of a very simple "ecosystem". This "ecosystem" is a
113 suitable and simple model to simulate and elucidate community metabolism. In the present
114 study, our aim was to understand the metabolic interactions between the two cell types within
115 the filament of *Anabaena* sp. PCC 7120 and to reveal the underlying reaction network
116 enabling such a relationship. We therefore reconstructed a genome-scale metabolic network
117 of *Anabaena* sp. PCC 7120 incorporating both cell types. The metabolic reconstruction
118 allowed us to perform an exhaustive computational analysis of possible exchange metabolites
119 and to rank exchange metabolites according to evolutionary optimality criteria, in particular
120 growth yield of the filament. To benchmark our reconstruction, we compared growth states of
121 *Anabaena* sp. PCC 7120 under both photoautotrophic and mixotrophic conditions, either
122 consuming a combined nitrogen source or growing diazotrophically. Our stoichiometric
123 model is represented using the systems biology markup language (Hucka et al., 2003) and is
124 being analysed by a constraint-based optimisation approach (Price et al., 2003; Steuer et al.,
125 2012). To our best knowledge, this reconstruction is the first extensively curated, genome-
126 scale model for *Anabaena* sp. PCC 7120. It is also the first complete reconstruction for

127 heterocyst metabolism and among the first attempts to simulate a simple multicellular
128 organism at genome-scale.

129 **Results and discussion**

130 **A manually curated stoichiometric model of *Anabaena* sp. PCC 7120**

131 The reconstruction process follows the protocol of (Thiele and Palsson, 2010) and is detailed
132 in the Materials and Methods. In brief, based on the available genome annotation (Kaneko et
133 al., 2001; Peterson et al., 2001) and reaction databases (Kanehisa et al., 2004; Caspi et al.,
134 2012), gene-protein-reaction (GPR) relationships were established. Elementally balanced
135 biochemical reactions were sorted into six intracellular compartments (cytosol, thylakoid
136 lumen, carboxysome, cytoplasmic membrane, thylakoid membrane and periplasmic space) in
137 order to simulate the growth of vegetative cells on a combined nitrogen source (single-cell
138 model).

139 The single cell reconstruction contains a total of 777 metabolites interconnected via 804
140 enzymatic and 14 spontaneous reactions, as well as 79 transport reactions between
141 intracellular compartments or the external space (Figure 1). Ninety-nine of the unique
142 metabolic reactions have not previously been reported in databases for *Anabaena* sp. PCC
143 7120 (Kanehisa et al., 2004; Caspi et al., 2012), but were acquired from the primary literature
144 for this organism. In addition, 60 reactions were associated with their gene candidates here for
145 the first time following a BLAST-based homology search. However, no candidate genes
146 could be identified for a total of 36 reactions of which 24 are essential for growth (see
147 Materials and Methods for more details).

148 The reconstruction was examined for orphan reactions, that is, reactions that are disconnected
149 from the remaining reactions. Such reactions (or reaction subsets) indicate misannotation or
150 insufficiently known pathways. Orphan reactions cannot carry metabolic flux and therefore
151 can either be kept or removed from the reconstruction without any observable impact on the
152 FBA solution. Here, a total of 98 orphan reactions were identified and moved to a separate
153 file for later analysis (Supplemental File S5), all being more than two reaction steps away
154 from the closest element within the network. Gaps that span two or less reaction steps were
155 resolved by finding gene associations to the missing steps, wherever possible. The gap-filling
156 process is detailed in the Materials and Methods section.

157 Along with the reconstructed biomass objective function (see below), biosynthesis routes for
158 the different carotenoids that accumulate in *Anabaena* sp. PCC 7120 were updated based on
159 literature (Albrecht et al., 1996; Takaichi et al., 2005; Takaichi and Mochimaru, 2007;

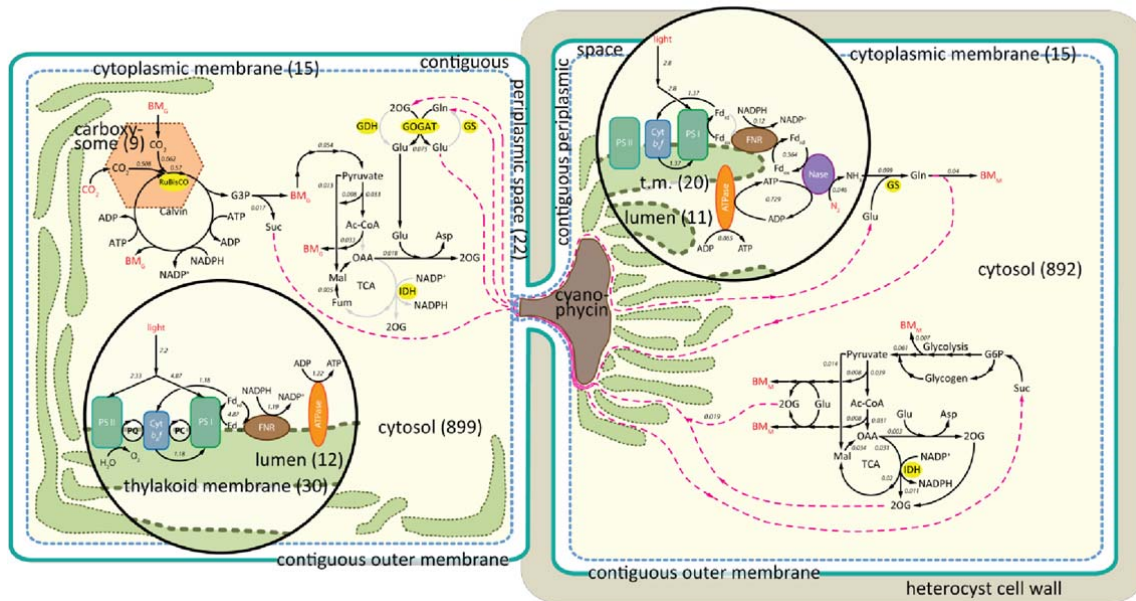


Figure 1. Compartments considered in the two-cell model. The filamentous structure of *Anabaena* sp. PCC 7120 under diazotrophic conditions is represented by two super-compartments (a vegetative cell and a heterocyst) sharing certain metabolites via exchange reactions (red dashed line). Black arrows and numbers in italic indicate main fluxes of diazotrophic growth. Super-compartments are divided into (sub)-compartments: both cells contain a cytosol (light yellow body), a thylakoid lumen (green bands), a thylakoid membrane (dark green dashes) and a cytoplasmic membrane (blue dashes) and share a contiguous periplasmic space (white space delimited by the cytoplasmic and outer membranes). The vegetative cell also carries carboxysomes (orange hexagon). The brown body in the heterocyst is the nitrogen storage cyanophycin, not a separate compartment on its own. Numbers in parentheses indicate the number of reactions (including transport) associated with that compartment. Cell types and compartments are not to scale.

160 Mochimaru et al., 2008; Graham and Bryant, 2009). The currently incomplete pathways for
 161 the synthesis of phycobilin, thiamine and molybdopterin in KEGG (Kanehisa et al., 2004)
 162 were also revised (Schluchter and Glazer, 1997; Gutzke et al., 2001; Ruiz et al., 2010; Biswas,
 163 2011). In addition, the sucrose metabolism of *Anabaena* sp. PCC 7120 was extended as
 164 compared to current database entries for this organism (Cumino et al., 2007; Marcozzi et al.,
 165 2009; Du et al., 2013). The reconstruction also includes a proposed pathway for the iron (III)-
 166 siderophore schizokinen based on the biosynthesis route of a similar siderophore, rhizobactin,
 167 from *Shinorhizobium meliloti* 1021 (Lynch et al., 2001; Nicolaisen et al., 2008; Malatinszky
 168 and Jones, unpublished). In order to aid the analysis of the model, a visual representation of
 169 the metabolic network was created (Supplemental File S6 and S7) using the software package
 170 Cytoscape (Shannon et al., 2003).

171

172 Two-cell model and biomass composition

173 In a separate model, the single-cell model is transformed into two super-compartments (Table
 174 I) to reflect the multicellular structure of the *Anabaena* sp. PCC 7120 filament under

175 diazotrophic conditions (two-cell model). The two-cell model contains a total of 1797
176 reactions including exchange between the two super compartments (see Figure 1 and Table I
177 for selected modifications to the heterocyst super-compartment). Transport reactions across
178 compartments and exchange between super compartments are assumed bidirectional,
179 independent of ATP and unconstrained in contrast to transport reactions to the external space
180 which are defined as ATP-driven, unless evidence for a different driving mechanism was
181 found in the literature (rows 1, 3 and 8 in Supplemental File S8).

182

183 The vast majority of the reactions exist in both the vegetative cell and the heterocyst, although
184 there are characteristic differences between the two super-compartments. Most importantly,
185 only the vegetative cell is able to perform oxygenic photosynthesis via linear
186 photophosphorylation, whereas only the heterocyst is capable of performing nitrogen fixation,
187 using cyclic photophosphorylation on photosystem I. Reactions responsible for oxygen
188 evolution in photosystem II were therefore deleted from the heterocyst super-compartment.
189 Similarly, the inactive RuBisCo-dependent carbon fixation was removed from the heterocyst,
190 although other carbon fixation mechanisms may still be active (see below). In addition,
191 nitrogen metabolism in the heterocyst lacks the expression of the GOGAT enzyme, but it may
192 have an active nitrogenase in place. The physiological differences between the two super-
193 compartments are listed in Table I, whilst the resulting differences in active reactions are
194 described in Supplemental File S5.

195 The terminally differentiated heterocyst does not grow or undergo cell division; therefore, the
196 objective function of the two-cell model is defined as the growth of the vegetative cell (row 5
197 in Supplemental File S8). To account for macromolecular turnover in the heterocyst (row 6 in
198 Supplemental File S8), the biomass reaction in this super-compartment is constrained to a
199 lower bound equal to 10% of the maximum biomass production in the vegetative cell (van
200 Bodegom, 2007). Moreover, both super-compartments include an artificial ATP hydrolysis
201 reaction to account for the energy requirement of growth-independent cell maintenance at a
202 fixed flux rate (row 7 in Supplemental File S8). This flux rate is equal to 10% of total ATP
203 consumption at maximum growth rate, similar to previous stoichiometric models (Feist et al.,
204 2007; Nogales et al., 2012; Knoop et al., 2013). In the initial two-cell model, the two super-
205 compartments are allowed to exchange four metabolites: sucrose (Schilling and Ehrnsperger,
206 1985; Cumino et al., 2007; Nürnberg et al., 2015), glutamine (Wolk et al., 1976; Thomas et
207 al., 1977; Picossi et al., 2005), glutamate (Martin-Figueroa et al., 2000) and 2-oxoglutarate
208 (Böhme, 1998) (row 12, Supplemental File S8). The transport reactions for these metabolites
209 are unconstrained, bidirectional and provide direct exchange between super-compartments

210 without the involvement of other compartments or the external space. In addition, any dilution
 211 occurring due to the size difference of the two cell types is not taken into account (rows 2 and
 212 9 in Supplemental File S8). At optimal growth, the heterocyst super-compartment was found
 213 to supply sufficient fixed nitrogen for the growth of exactly 7.6 new vegetative cells, based on
 214 the nitrogen content of the vegetative cell in the biomass equation. This calculation
 215 determines the maximum number of growing vegetative cells a single heterocyst can support.
 216 However, already existing vegetative cells adjacent to the heterocyst require less nitrogen to
 217 remain functional, increasing this ratio to the range observed experimentally (i.e. ten to
 218 twenty vegetative cells per heterocyst). At such ratios the predicted growth rate drops
 219 gradually, reaching about 46% of the maximal rate when a single heterocyst sustains exactly
 220 twenty vegetative cells. It is worth noting that the growth rate predicted by the model does not
 221 predict actual cell number, but biomass accumulation rate. Therefore, in our reconstruction we
 222 represented the *Anabaena* sp PCC 7120 filament as a single vegetative super-compartment
 223 and a single heterocyst super-compartment, denoted as the two-cell model in the following
 224 (Figure 1 and row 4 in Supplemental File S8).

225 Figure 1 summarizes the main metabolic fluxes concerning carbon and nitrogen metabolism
 226 in the two-cell model under diazotrophic growth conditions. The vegetative cell fixes carbon
 227 via the Calvin cycle driven by photosynthesis and produces an excess of sucrose from
 228 glyceraldehyde 3-phosphate and an excess of glutamate synthesized by the GOGAT enzyme.
 229 The primary source of glutamate is internally recycled 2-oxoglutarate and glutamine of
 230 heterocyst origin. The excess sucrose and glutamate are exchanged for glutamine and 2-
 231 oxoglutarate from the heterocyst. Glutamine is derived from glutamate by incorporating
 232 ammonia from heterocystous nitrogen fixation to glutamate from the vegetative cell. Energy
 233 (ATP) and electron (reduced ferredoxin) requirements of the nitrogenase reaction are mainly
 234 covered by cyclic photophosphorylation at photosystem I. The rest of the energy is provided
 235 by degrading sucrose from the vegetative cell, and spending its carbon content on cellular
 236 maintenance (Figure 1).

237

238 **Table I. Major differences between the two super-compartment (cell types) in the *Anabaena* sp. PCC 7120 model**

vegetative cell	heterocyst
photosynthesis (PSI and PSII) ^a	cyclic photophosphorylation (PSI only) ^a (Wolk et al., 2004)
carboxysomes and RuBisCO ^b	neither carboxysomes nor an active RuBisCO ^b (Madan and Nierzwicki-Bauer, 1993; Valladares et al., 2007)
no nitrogen fixation	nitrogen fixation (nitrogenase)
GS-GOGAT cycle ^c	Fd-GOGAT missing ^c (Martin-Figueroa et al., 2000)
FNR at PSI produces NADPH ^d	FNR produces red. FdxH for nitrogenase ^d (Razquin et al., 1996)
<i>cox1</i> cytochrome c oxidase	contains <i>cox2</i> and <i>cox3</i> only (Valladares et al., 2003)

239 ^a PSI: photosystem I; PSII: photosystem II

240 ^b RuBisCO: ribulose-1,5-bisphosphate carboxylase/oxygenase

241 ^c GS: glutamine synthetase; GOGAT: glutamine-oxoglutarate aminotransferase; Fd-: Ferredoxin-dependent
 242 ^d FNR: ferredoxin-NADP⁺ reductase; FdxH: heterocyst-specific ferredoxin
 243

244 There is very little information on the exact composition of *Anabaena* sp. PCC 7120 biomass
 245 in the literature (Table II). Therefore, the biomass equation constructed for *Synechocystis* sp.
 246 PCC 6803 by (Nogales et al., 2012) and adjusted by (Knoop et al., 2013) was used here and
 247 adapted to *Anabaena* sp. PCC 7120, complemented by sparsely available analytical data
 248 (Table II). Vegetative cells and heterocysts were assumed to share the same fractional
 249 composition comprising DNA, RNA, proteins, pigments, lipids, cell wall, inorganic ions and
 250 the metabolic pool (row 10, Supplemental File S8). The fractional composition given in
 251 (Nogales et al., 2012) was left unchanged; however, some of the fractions were recalculated if
 252 data was available (Table II, row 11 in Supplemental File S8). The impact of variation in the
 253 biomass composition on the predicted growth rate was simulated and the results are shown in
 254 Supplementary Figure S9. Even a +/- 20% variation in any one component did not influence
 255 the predicted growth rate by more than +/- 3%.

256

257 **Table II. Biomass composition used in the model.** Fractional composition was adopted from the *Synechocystis* sp. PCC
 258 6803 model developed by (Nogales et al., 2012; Knoop et al., 2013). The definition and the reaction formula of the different
 259 fractions were adapted for *Anabaena* sp. PCC 7120, wherever specific analysis data was available.

Fraction	Source of data and reference
Pigments	Analysis of carotenoid composition (Takaichi et al., 2005; Takaichi and Mochimaru, 2007; Mochimaru et al., 2008; Graham and Bryant, 2009)
DNA	Base abundance calculated from the genome sequence (Kaneko et al., 2001)
RNA	Base abundance calculated for annotated genes and weighted by RNAseq abundance (Kaneko et al., 2001; Flaherty et al., 2011)
Proteins	Amino acid abundance calculated and weighted by RNAseq abundance (Kaneko et al., 2001; Flaherty et al., 2011)
Lipids	Adopted from <i>Synechocystis</i> sp. PCC 6803 (Nogales et al., 2012; Knoop et al., 2013)
Cell wall	Adopted from <i>Synechocystis</i> sp. PCC 6803
Inorganic ions	Adopted from <i>Synechocystis</i> sp. PCC 6803
Pool fraction	Adopted from <i>Synechocystis</i> sp. PCC 6803 ^c

260 ^c No genes could be identified for the biosynthesis of spermidine (Jantaro et al., 2003; Incharoensakdi et al., 2010).

261

262 **Computational characterization of the reconstructed metabolic model**

263 Simulations were run using the two-cell model under photodiazotrophic conditions with
 264 glutamate, glutamine, 2-oxoglutarate and sucrose as possible exchange metabolites, and
 265 bicarbonate, molecular dinitrogen and light as only external substrates. The uptake of the
 266 external substrates was constrained to upper bounds of 10 mmol g dry weight (DW)⁻¹ h⁻¹ each.
 267 Figure 2 shows the relationship between light intensity and bicarbonate uptake. The maximal
 268 growth rate is reached at 10 mmol g DW⁻¹ h⁻¹ photon flux (the upper bound) and the
 269 bicarbonate uptake rate of 0.68 mmol g DW⁻¹ h⁻¹.

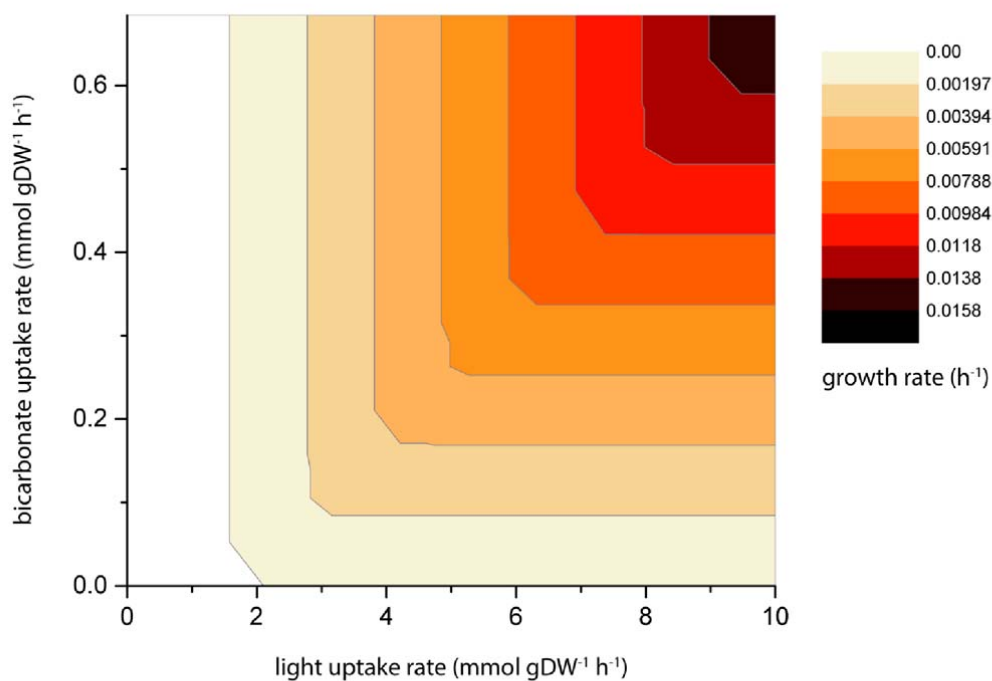


Figure 2. Predicted optimal growth rates of *Anabaena* sp. PCC 7120 as a function of light and bicarbonate. Darker colours represent higher growth rates (see legend on the right). Photon requirement of cell maintenance is represented by a white area on the left side of the contour plot.

270

271 To obtain insight into the properties of the two-cell model, and to test to what extent model-
 272 based predictions coincide with known metabolic exchange fluxes, we evaluated the two-cell
 273 model under photodiazotrophic conditions (Figure 3).

274

275 The minimum photon requirement to cover non-growth associated maintenance costs without
 276 supporting growth (x-intercept) is shown in Figure 3A. This requirement is equal to a photon
 277 flux of 6 mmol g DW⁻¹ h⁻¹, when light is harvested by the vegetative cell only (solid blue
 278 line). At the upper bound of the vegetative cell's photon uptake (10 mmol g DW⁻¹ h⁻¹) the
 279 growth rate is 0.006 h⁻¹ (Figure 3A, solid blue line and y-intercept on panel B) that increases
 280 up to the maximum (0.0144 h⁻¹) by the heterocyst's contribution to light harvesting. In the
 281 case when both super-compartments harvest light (dotted red line) the energy contribution by
 282 the heterocyst lowers the requirement from the vegetative cell by about 2.3 mmol g DW⁻¹ h⁻¹.
 283 This contribution by the heterocyst via cyclic photophosphorylation saturates at approx. 4.2
 284 mmol g DW⁻¹ h⁻¹, over which the proton gradient through the thylakoid membrane is
 285 replenished by secondary reactions in the electron transport chain without the synthesis of
 286 additional ATP (Figure 3B). In contrast, light or carbon uptake by the heterocyst alone cannot

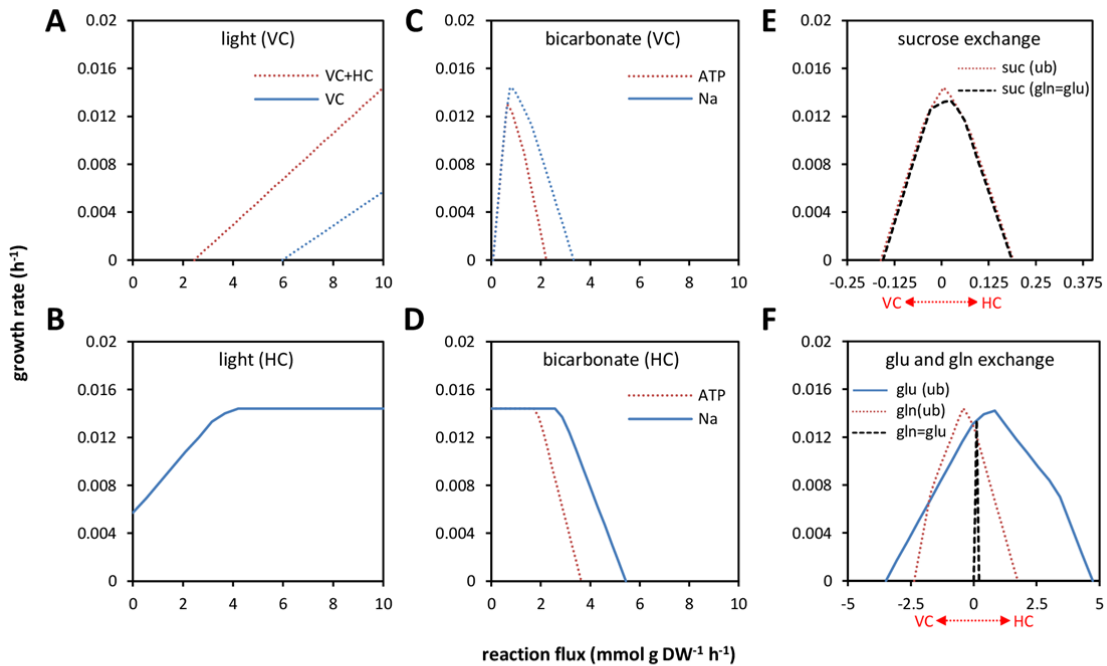


Figure 3. Growth rates predicted as a function of different transport reactions under diazotrophic conditions. (A) Impact of light availability on growth rate when both cell types (dotted red line) or only the vegetative cell (solid blue line) harvest photons. **(B)** Photon uptake by the heterocyst in combination with optimal light harvesting in the vegetative cell. **(C)** Bicarbonate uptake by the two transport reactions (sodium symport, solid blue line; active transport, dotted red line) in the vegetative cell. **(D)** Bicarbonate uptake by the heterocyst. **(E)** Exchange of sucrose if the glutamine-to-glutamate ratio is unbound (red dotted line) or fixed to 1 (black dashed line). **(F)** Exchange of glutamate and glutamine at ratios fixed to 1 (black dashed line) or left unbound (solid blue and dotted red lines). Red double arrows on E and F show the direction of exchange. VC: vegetative cell; HC: heterocyst.

287 support growth of the vegetative cell (data not shown). On the other hand, any of the two
 288 bicarbonate transporters in the vegetative cell can provide sufficient carbon for growth,
 289 although the maximum rate is lower for the ATP-driven transport (Figure 3C, dotted red line).
 290 Forcing bicarbonate uptake over the optimum, however, both transport reactions have a
 291 negative effect on growth as light becomes limiting (Figure 3C, both lines). According to
 292 Figure 3D, maximal growth can be achieved even at zero bicarbonate uptake by the
 293 heterocyst, suggesting that the vegetative cell alone can fix sufficient amount of carbon (via
 294 RuBisCO in the carboxysome) to reach maximum growth rate. Moreover, if bicarbonate
 295 uptake in the heterocyst is enforced (Figure 3D, both curves), the carbon is not utilized for
 296 growth (straight horizontal lines on the left side of each curve), but rather recycled via the C₄
 297 dicarboxylic acid cycle and released as carbon dioxide (not shown here). The recycling
 298 capacity depletes around 1.8 and 2.6 mmol g DW⁻¹ h⁻¹ bicarbonate over the active transport
 299 and the symport, respectively. Nonetheless, it is still unclear whether in reality heterocysts
 300 utilize this C₄ route to fix their own carbon (Popa et al., 2007); although cyanobacteria have
 301 been described to assimilate about 20% of the total fixed CO₂ in the form of C₄ acids
 302 (Owtrim and Colman, 1988; Luinenburg and Coleman, 1992, 1993). Notably, experimental

303 evidence suggests that the main source of carbon for heterocysts is likely to be sucrose
304 (Böhme, 1998; Martin-Figueroa et al., 2000; Kumar et al., 2010; Nürnberg et al., 2015). In
305 contrast, the model predicts a very low flux for sucrose at the optimal growth rate (Figure 3E,
306 red dotted line). In the same simulation, glutamate is transferred to the heterocyst at a two-
307 fold higher rate than that of glutamine, moving in the reverse direction. This is possible
308 because glutamine and glutamate exchange were optimized as independent reactions and
309 suggests that glutamate is partially utilized as a carbon source in the heterocyst. However,
310 sucrose becomes the primary source of carbon in the heterocyst (also increasing its flux by 4-
311 times), if the glutamine-glutamate exchange ratio is fixed to 1, while the growth optimum
312 decreases by only about 7% (Figure 3E and F, dashed black lines; row 13 in Supplemental
313 File S8). Further tests of the model comparing growth rates on different carbon and nitrogen
314 sources can be found in Supplemental File S10.

315

316

317 **Experimental evaluation of model predictions on carbon source utilisation by the** 318 **single-cell model**

319 Experimental and predicted mixotrophic growth rates on a variety of carbon sources were
320 compared relative to autotrophic growth on bicarbonate, using nitrate as the sole nitrogen
321 source. In the presence of nitrate no heterocysts are expected to form, the following growth
322 rate calculations were therefore performed using the single-cell model. Tested carbon sources
323 included bicarbonate, urea, sugars (glucose, fructose, sucrose and maltose), a sugar alcohol
324 (glycerol), fermentation products (pyruvate and acetate), amino acids (glutamate, glutamine
325 and proline) and a polyamine (putrescine). For comparative reasons, each uptake reaction was
326 assumed to hydrolyse one molecule of ATP and was constrained to transport equal moles of
327 carbon with each substrate (row 14 in Supplemental File S8). Light harvesting, bicarbonate
328 and nitrate uptake were constrained to an upper bound of 10 mmol g DW⁻¹ h⁻¹. The two
329 datasets of relative growth rates in exponential phase are shown in Figure 4.

330

331 Most data points show a good fit to the trend, except for glycerol, some sugars and glutamine.
332 The latter amino acid supported the second highest growth rate in the experiments, exceeded
333 only by glucose. In contrast, simulated growth rate on glutamine was just above the control
334 bicarbonate. Interestingly, the model predicted the same growth rate for glutamine and
335 glutamate when ammonia excretion was allowed, resulting in a 2.6-fold increase of growth
336 rate on glutamine. This suggests that the two-fold higher molar nitrogen content of glutamine

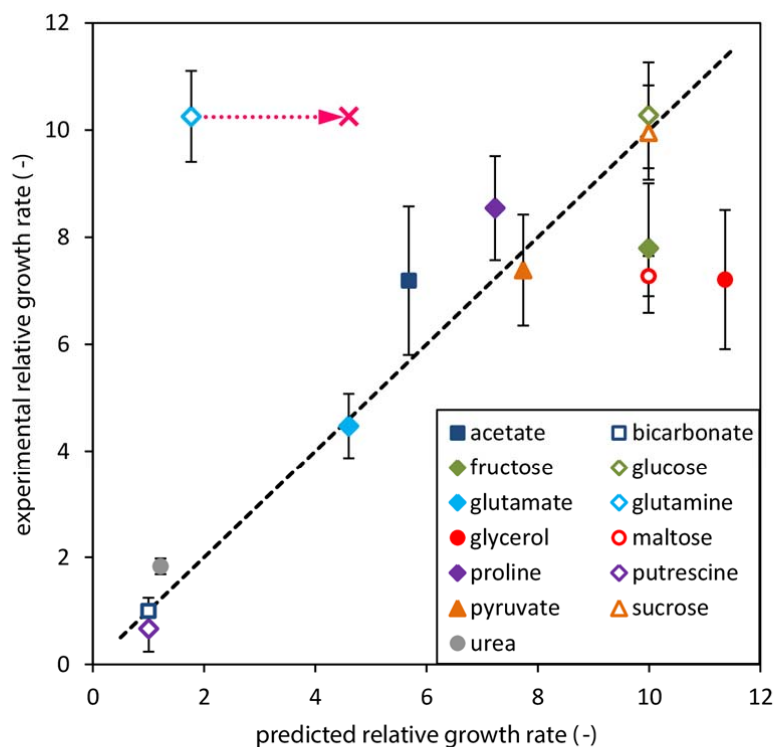


Figure 4. Correlation between experimental and predicted mixotrophic growth rates in the exponential phase on twelve different carbon sources, relative to autotrophic growth on bicarbonate. The pink cross and dotted arrow show the shift in predicted growth rate on glutamine if ammonia is being excreted. The black dashed line highlights the correlation between experimental and computational datasets. Error bars depict \pm standard deviation of three biological replicates.

337 makes this amino acid a stoichiometrically unfavoured substrate compared to glutamate,
 338 which can only be overcome by the removal of excess nitrogen. By excreting nitrogen the
 339 model compensates for the suboptimal C/N ratio of glutamine and shifts the intracellular C/N
 340 ratio to the same level as with glutamate (Figure S3 in Supplemental File S10, green squares).
 341 The adjustment via addition of ammonia excretion only brings predicted glutamine halfway to
 342 experimental levels and the contrasting difference between the two datasets therefore remains
 343 incompletely explained. In addition, excretion of ammonia under diazotrophic conditions has
 344 not yet been observed experimentally. However, it may be possible that the excess nitrogen is
 345 being deposited to nitrogen storage (i.e. cyanophycin), rather than being lost via excretion.
 346 Among the sugar compounds, datasets for glucose and sucrose showed good correlation,
 347 whilst fructose and maltose underperformed in wet-lab experiments. In fact, the four sugars
 348 showed essentially the same growth rate in simulations, due to high stoichiometric similarities
 349 between the metabolic pathways of these substrates (further discussed for Figure S1 in
 350 Supplemental File S10). *In silico*, growth on glycerol resulted in the highest growth rate,
 351 whereas experimentally growth on glucose achieved the highest rate. Glucose and glycerol are
 352 both metabolised to glyceraldehyde 3-phosphate (GA3P), but via two different pathways. We
 353 note that sub-optimal growth on glycerol as sole carbon source, as compared to predictions

354 using an FBA-based model, was also previously observed for *Escherichia coli* K-12 (Ibarra et
355 al., 2002). For *E. coli*, adaptive evolution resulted in an increased growth rate on glycerol, in
356 good agreement with model-predicted values (Ibarra et al., 2002). For the present model, a
357 variety of reasons might be responsible for the discrepancy, such as the thermodynamic
358 properties of the dehydrogenation step to dihydroxyacetone phosphate, or lack of appropriate
359 NAD(P)(H) balancing. Nonetheless, the results in Figure 4 show that the constraint-based
360 model provides a reasonable prediction of mixotrophic growth rates on different carbon
361 sources, thereby justifying the use of the stoichiometric model to evaluate the feasibility and
362 optimality of potential exchange reactions in more detail.

363

364

365 **Stoichiometric evaluation of metabolite exchange within the filament**

366 Following the characterization of the curated single-cell model, we sought to obtain insight
367 into the stoichiometric optimality of the metabolic exchange between vegetative cells and
368 heterocysts. Notably, a systematic analysis of the stoichiometric and energetic implications of
369 different metabolites in intra-species cellular exchange is challenging to carry out
370 experimentally, whilst being feasible *in silico*. From previous studies, sucrose was proposed
371 to act as the sole source of electrons and carbon for heterocysts (Curatti et al., 2002; Golden
372 and Yoon, 2003; Cumino et al., 2007) and glutamine was suggested to serve as a nitrogen
373 carrier and glutamate as carbon skeleton for ammonia incorporation (Flores and Herrero,
374 2010; Kumar et al., 2010). In addition, the lack of glutamine oxoglutarate aminotransferase
375 (GOGAT) in heterocysts was postulated to result in the accumulation and subsequent
376 transport of 2-oxoglutarate into the vegetative cells (Böhme, 1998; Martin-Figueroa et al.,
377 2000). These compounds and other central carbon metabolites including some amino acids
378 that may be involved in intercellular nitrogen exchange (Montesinos et al., 1995) were
379 included as potential exchange metabolites in the two-cell model. In addition to amino acids,
380 ammonia was also investigated as an alternative carrier of nitrogen. Therefore, in total, twelve
381 different metabolites were considered as exchange metabolites and all possible combinations
382 were comprehensively evaluated with respect to the predicted maximal growth rate, resulting
383 in 4096 combinations. Earlier simulations suggested that the ratio of glutamine and glutamate
384 exchange may be constrained to unity (Figure 3) and therefore this case (as an additional
385 constraint) was also included. Results were plotted as a distribution chart against the number
386 of exchange reactions involved in each solution (Figure 5A). Selected exchange metabolite
387 combinations (Figure 5B) showing the highest growth rates by involving the least number of

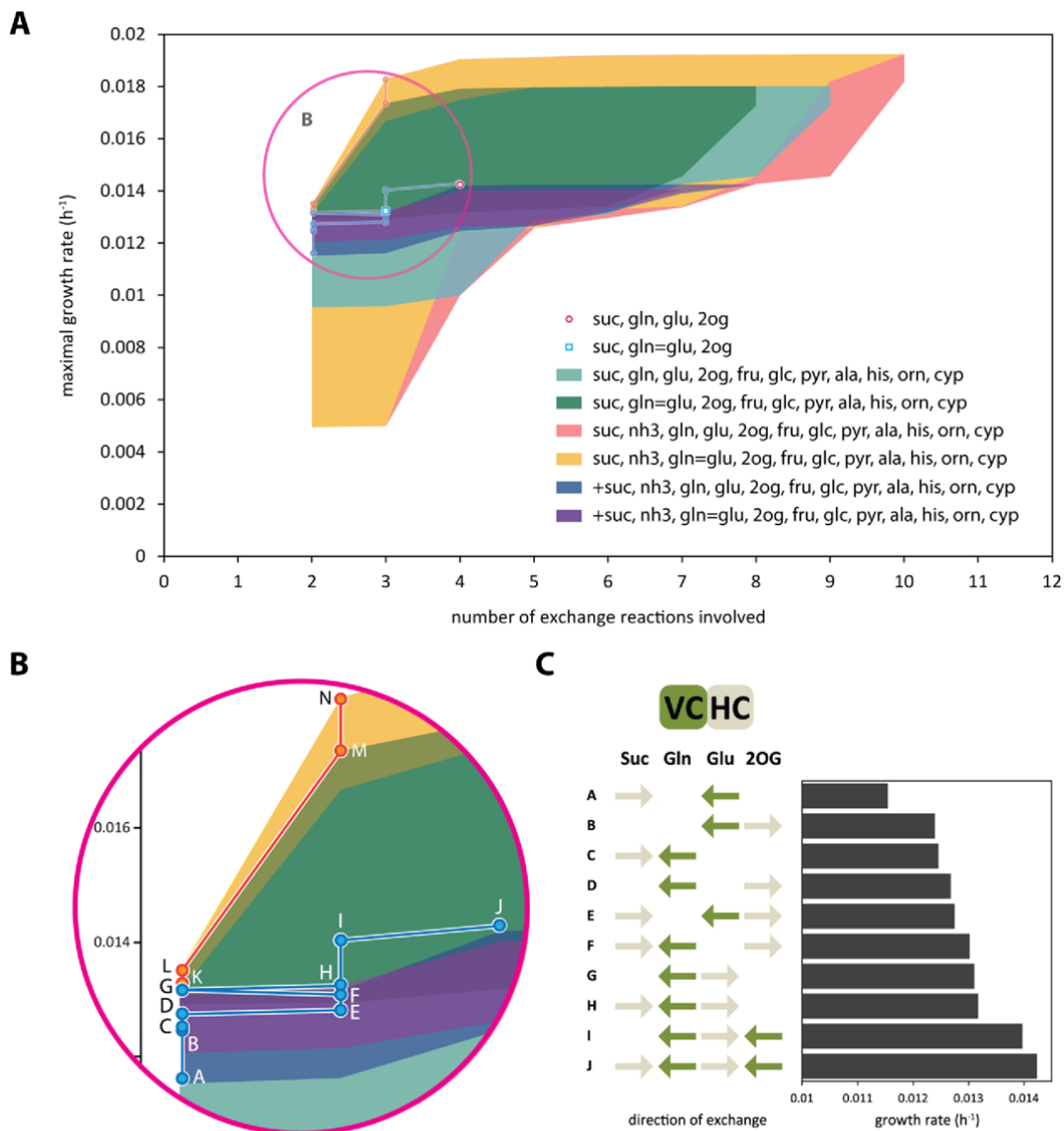


Figure 5. Predicted growth rates in response to the number of intercellular exchange reactions. (A) Each coloured area represents the distribution of non-zero solutions with a different set of exchange reactions. In case of yellow and green glutamine to glutamate ratio was fixed to 1. The ratio was unbound for cases red and teal. Yellow and red areas evaluate the effect of ammonia exchange. Blue and purple areas highlight solutions where sucrose was consumed by the heterocyst. The growth rate for the four exchange metabolites suggested in the literature (i.e. sucrose, 2-oxoglutarate, glutamate and glutamine) is highlighted by a red circle (glutamine to glutamate ratio unbound) and a blue square (ratio fixed to 1). All simulations were performed using the two-cell model. Abbreviations: suc: sucrose, nh3: ammonia, gln: L-glutamine, glu: L-glutamate, 2og: 2-oxoglutarate, fru: fructose, glc: glucose, pyr: pyruvate, ala: L-alanine, his: L-histidine, orn: L-ornithine and cyp: cyanophycin monomer. (B) Zoomed-in section from panel A showing growth rates for selected exchange metabolite combinations. Letters refer to cases on panel C and the corresponding panels on Figure 6 and 7. (C) Combination of a maximum of four reactions exchanging sucrose (Suc), glutamine (Gln), glutamate (Glu) or 2-oxoglutarate (2OG). Arrows indicate the metabolites exchanged and the direction of the exchange (uptake by the vegetative cell and the heterocyst is represented by green and beige colours, respectively). Black bars show growth rate in each case.

388 exchange metabolites are further evaluated on Figure 6 and Figure 7, highlighting the major
 389 metabolic pathways and reactions involved in the solution.

390

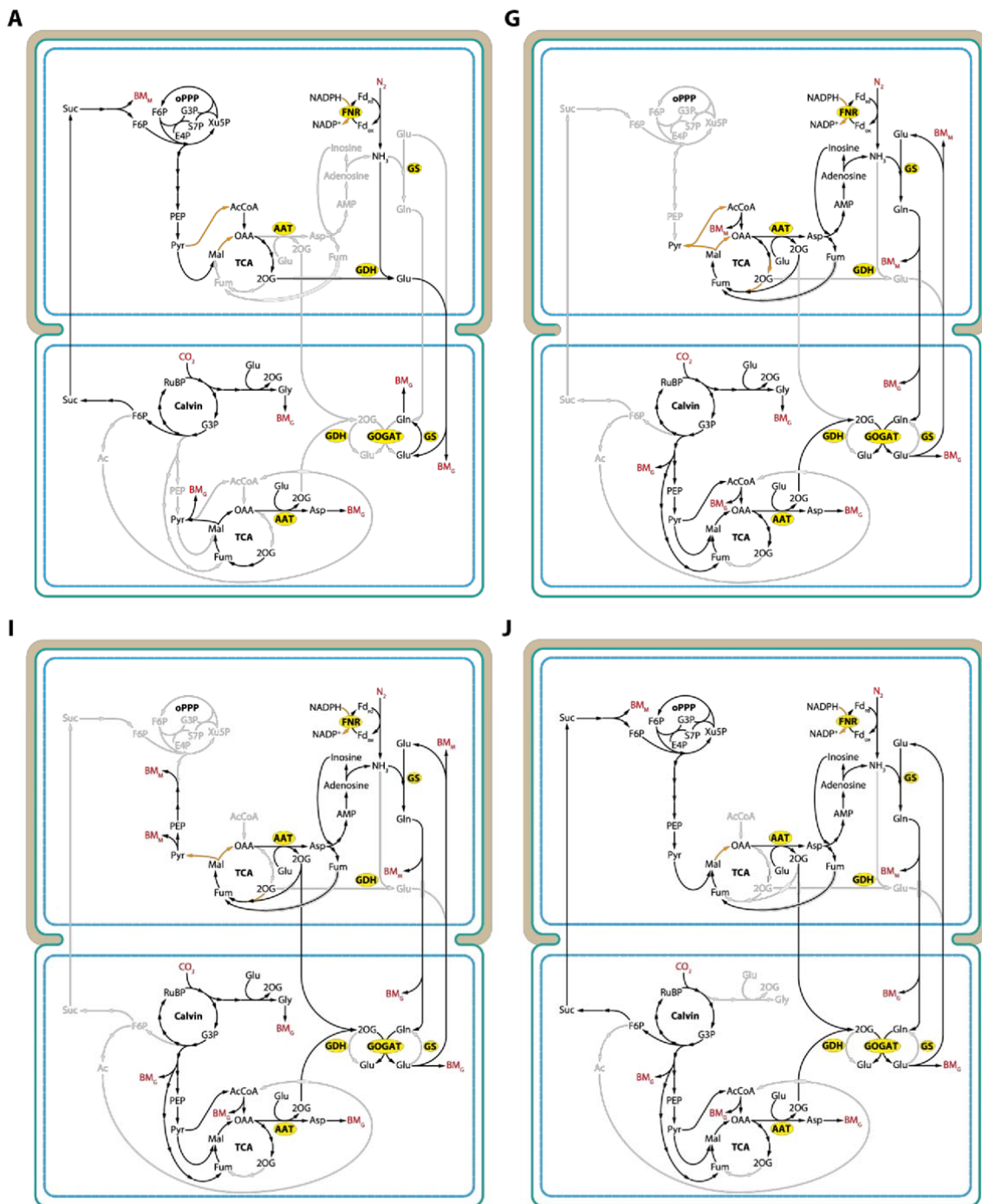


Figure 6. Main metabolic fluxes connecting exchange metabolites sucrose, glutamine, glutamate and 2-oxoglutarate. Panels are labelled according to cases on Figure 5B (blue dots) and C, and show increasing growth rates from (A) to (J). Exchange reactions are as follows: (A) +Suc -Glu; (G) +Glu -Gln; (I) +Glu -Gln -2-og; (J) +Suc +Glu -Gln -2-og. Ratio of Glu to Gln was unbound. Compounds in red indicate a sink or uptake of an external metabolite. Orange arrows in the heterocyst highlight reactions providing electrons (NADPH) for nitrogenase. BM_G : biomass (growth), BM_M : biomass (maintenance). Enzyme names are highlighted in yellow. Upper cells: heterocysts, lower cells: vegetative cells.

391 None of the exchange metabolites investigated here, including ammonia and glutamine, was
 392 able to individually allow growth of the filament (Figure 1). Any combination of two
 393 exchange metabolites did not result in maximal growth rates. As the best-ranked combination
 394 of two exchange reactions, export of ammonia and import of alanine (from the heterocysts

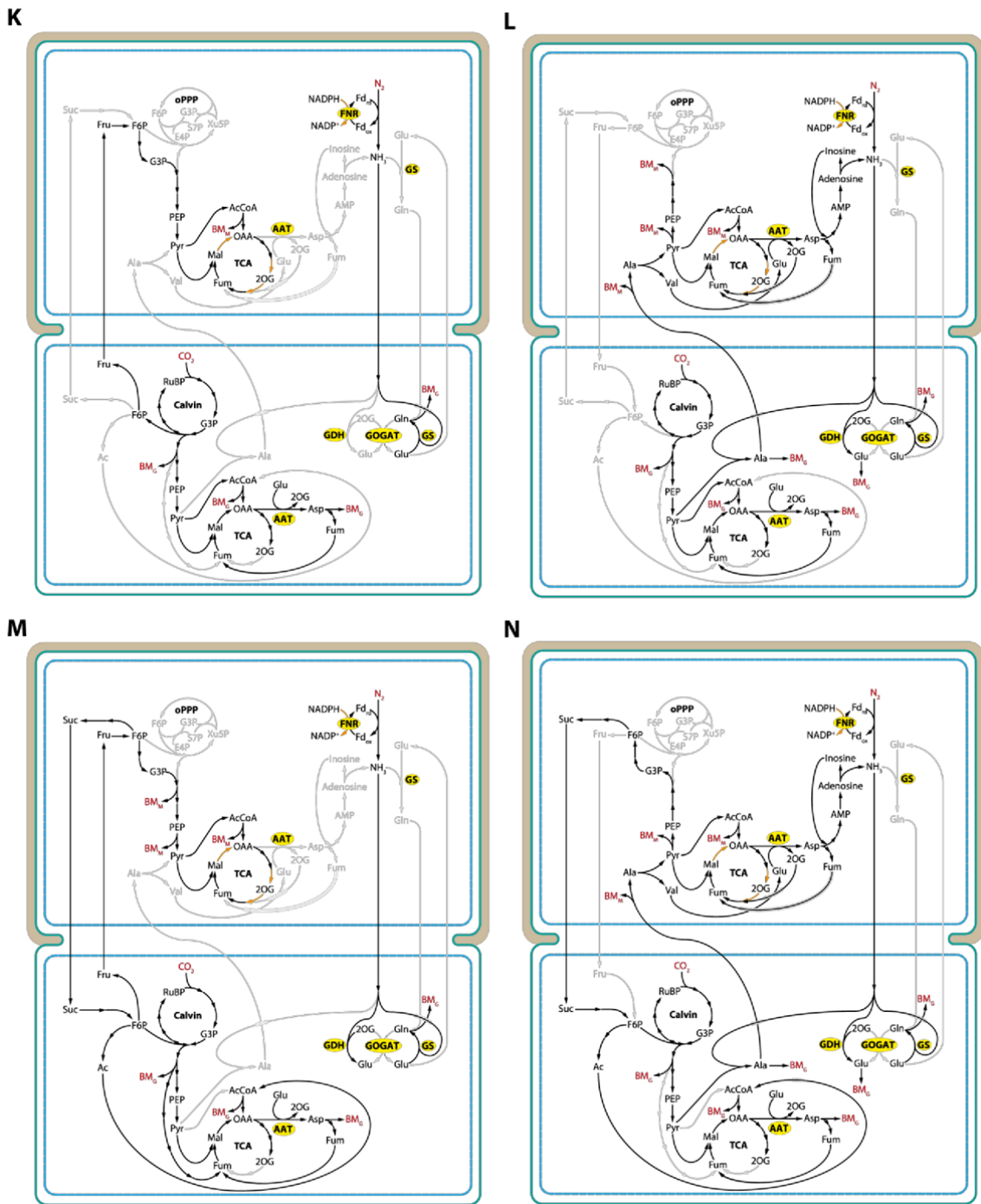


Figure 7. Main metabolic fluxes connecting exchange metabolites sucrose, fructose, alanine and ammonia. Panels are labelled according to cases on Figure 5B (red dots), and show increasing growth rates from (K) to (N). Exchange reactions are as follows: **(K)** +Fru -NH₃. **(L)** +Ala -NH₃. **(M)** +Fru -Suc -NH₃. **(N)** +Ala -Suc -NH₃. Ratio of Glu to Gln was unbound. Compounds in red indicate a sink or uptake of an external metabolite. Orange arrows in the heterocyst highlight reactions providing electrons (NADPH) for nitrogenase. BM_G: biomass (growth), BM_M: biomass (maintenance). Enzyme names are highlighted in yellow. Upper cells: heterocysts, lower cells: vegetative cells.

395 perspective) resulted in 70% of the maximal growth rate (Figure 5B, case L). Moreover,
 396 although a total of twelve metabolites were allowed to exchange, no more than ten were ever
 397 chosen in any combination by the model to provide a feasible solution and non-zero growth.
 398 The maximal growth rate was reached by combinations of seven reactions with only slight

399 improvements over the combinations of four reactions. Flux distributions were, to variable
400 extent, different in each case.

401 At maximal growth rates, regardless of the number of exchange reactions involved or the
402 glutamine-glutamate ratio, alanine was consumed by the heterocyst and nitrogen was
403 transferred as ammonia. Furthermore, sucrose was produced and excreted, rather than being
404 consumed, by the heterocyst. When sucrose was consumed (blue and purple areas),
405 glutamine, glutamate and 2-oxoglutarate were transported as suggested by literature.
406 However, the growth rate was on average 30% higher if sucrose was exported, independent of
407 the glutamine-glutamate ratio. Ammonia was favoured over glutamine for the transfer of
408 nitrogen throughout the simulation, increasing growth rates by 5–7% when the glutamine to
409 glutamate ratio was fixed (Figure 5A, yellow area) and by 3–7% when it was unbound (red
410 area). When only four reactions were allowed, inclusion of ammonia increased growth rate by
411 38% over the reference (blue square) if glutamine to glutamate ratio was fixed and by 34%
412 over the reference (red circle) if unbound. Those four exchange metabolites suggested in
413 literature, i.e. sucrose (Suc), glutamine (Gln), glutamate (Glu) and 2-oxoglutarate (2-og) were
414 evaluated in more detail by looking at the flux distribution of each possible combination
415 individually (Figure 5B blue line and C). Only ten out of the sixteen exchange combinations
416 allowed growth, with +Suc and –Glu giving the lowest growth rate (in the following, + and –
417 signs preceding metabolite names denote uptake and excretion by the heterocyst,
418 respectively). In this case (Figure 6 case A) an incomplete TCA cycle is driven by sucrose
419 originated from the vegetative cell to produce 2-oxoglutarate by isocitrate dehydrogenase
420 (IDH) and then convert it to glutamate by glutamate dehydrogenase (GDH), incorporating
421 ammonia fixed by nitrogenase. Eventually, electrons required by nitrogenase are also derived
422 partially from sucrose via pyruvate. The glutamate produced is transferred back to the
423 vegetative cell to serve as a source of assimilable nitrogen. This nitrogen is directly
424 incorporated into different amino acids and finally, biomass (Figure 6 case A). Growth rate
425 increases in ascending order when –Glu +2-og (Figure 5C case B), +Suc –Gln (case C) and –
426 Gln +2-og (case D) are combined. Interestingly, pairing glutamine with glutamate (–Gln
427 +Glu, case G) improves growth rate the most significantly among all the combinations of two
428 reactions. About 78% of glutamate is used to incorporate ammonia into glutamate by
429 glutamine synthetase (GS) and is sent back to the vegetative cell as glutamine. The rest of the
430 glutamate fuels the second half of the TCA cycle via aspartate transaminase (AAT). In the
431 vegetative cell GOGAT instead of GS becomes active and produces Glu for filament growth
432 and for the heterocyst. The 2-og required by GOGAT is the product of a broken TCA cycle
433 and AAT converting oxaloacetate to aspartate in the vegetative cell (Figure 6 case G).

434 Addition of 2-og exchange increases growth rate by another 7% (Figure 5C) allowing the
435 heterocyst to recycle some of the glutamate and return it to the vegetative cell as 2-og,
436 independent of the exchange of nitrogen (Figure 6 case I). This carbon transfer from the
437 heterocyst in the form of 2-og becomes higher if Suc is also allowed to exchange (case J). In
438 this case, sucrose is used to run only the second half of the TCA cycle without consuming any
439 2-og in the pathway and sending the majority of 2-og to the vegetative cell. In the absence of
440 an active first half of the TCA cycle the primary source of electrons for nitrogenase becomes
441 malate dehydrogenase, also involving transhydrogenase (Figure 6 case J, orange arrow in the
442 upper cell). Transhydrogenase shuffles electrons from NADH produced in the malate
443 dehydrogenase reaction to NADPH. In all cases discussed above (Figure 6 case A, G, I and J),
444 the main provider of reduced ferredoxin for nitrogenase is ferredoxin-NADP⁺ reductase
445 (FNR) transferring electrons from NADPH to ferredoxin.

446

447 The highest increase in growth rate due to the addition of one more reaction occurred from
448 two to three (Figure 5B, red line and circles) using ammonia as the carrier of fixed nitrogen.
449 The lowest growth rate among those with only two reactions was achieved when ammonia
450 exchanged for fructose (Fru, Figure 7 case K). Ammonia in the vegetative cell is assimilated
451 solely by GS and the resulting Gln is incorporated to other amino acids and biomass. The
452 source of Fru is the Calvin cycle and Fru is converted to pyruvate in the heterocyst. Pyruvate
453 eventually forms oxaloacetate to maintain the TCA cycle providing NADPH for the reverse
454 reaction at FNR producing reduced ferredoxin for nitrogenase (Figure 7 case K). As discussed
455 above, exchange of ammonia for alanine (Figure 7 case L) gave the highest growth rate
456 among all the combinations of only two reactions. Ammonia in this case is assimilated by
457 both GS and GDH in the vegetative cell with significantly higher contribution from the first
458 enzyme, while GOGAT remains inactive. In addition, ammonia is also incorporated to
459 pyruvate forming alanine that is then transferred back to the heterocyst. The nitrogen carried
460 by alanine is converted eventually back to ammonia via aspartate and adenosine.

461 Allowing exchange of sucrose, growth rate improves by about 30% (case M, Figure 5B)
462 compared to the case when only +Fru and -NH₃ were exchanging (case K). Also, the model
463 increases Fru exchange 100-times and sets Suc flux accordingly. In other words, Fru and Suc
464 exchange fluxes are closely equivalent for carbon content, except for some Fru consumed by
465 the heterocyst to run the TCA cycle. Stoichiometrically, the net outcome of this cycling of Fru
466 to Suc in the heterocyst and Suc to Fru in the vegetative cell is ultimately one mole of ATP
467 for every mole of Fru by the reverse reaction of fructokinase in the vegetative cell. It is
468 unclear, however, if such metabolite concentrations to shift the fructokinase reaction kinetics

469 to the direction of ATP generation can ever occur in a vegetative cell. It is also worth noting,
470 in most cases the model favoured, when available, exchange of carbon sources other than
471 sucrose, or transported sucrose towards the vegetative cell. In case of the fastest growing
472 among those using only three reactions (case N), the increase in growth rate due to the
473 addition of Suc exchange is about 36% compared to case L (Figure 5B), which uses only two
474 reactions (+Ala -NH₃). Similar to that, case N has no active GOGAT in the vegetative cell
475 while actively assimilating ammonia via GS, GDH and alanine dehydrogenase producing
476 alanine. The higher exchange rate of alanine compared to case L increases the flux over the
477 second half of the TCA cycle as well (generating more reducing equivalents), allowing higher
478 nitrogen fixation rate and ultimately, more vegetative cell biomass. The carbon content of Ala
479 is recycled through pyruvate and fructose 6-phosphate, and sent back to the vegetative cell in
480 the form of sucrose.
481

482 **Conclusion**

483 As yet, stoichiometric reconstructions of cyanobacterial metabolism have mainly focused on
484 unicellular non-diazotrophs (Saha et al., 2012; Knoop et al., 2013) or non-heterocystous
485 diazotrophs (Resendis-Antonio et al., 2007; Saha et al., 2012; Vu et al., 2012). Here, we
486 presented a curated genome-scale stoichiometric model of a filamentous heterocystous
487 nitrogen-fixing cyanobacterium with two distinct cell-types.

488 During the reconstruction process sixty genes and proteins have been newly annotated and
489 associated with a metabolic function based on sequence homology and, in a few cases,
490 experimental observations. In addition, a total of thirty-six gene candidates have been
491 proposed to fill essential and non-essential metabolic gaps in the biochemical network of
492 *Anabaena* sp. PCC 7120. Moreover, the extensive manual curation of every reaction in the
493 reconstruction and the design of a detailed interactive network map (Supplemental File S6)
494 allowed us to identify and eliminate inconsistent reactions that represented roughly 30% of
495 the total reactions found in current metabolic databases for this organism.

496 The model correctly predicted the vegetative cell to heterocyst ratio under diazotrophic
497 conditions showing that the heterocyst super-compartment (a single heterocyst) can supply the
498 formation of 7.6 vegetative cells at maximum growth rate. This ratio was increased at the
499 expense of vegetative cell growth rate, decreasing growth rate to 46% percent of the
500 maximum to sustain twenty vegetative cells by a single heterocyst. Nitrogen uptake rate in the
501 heterocyst was not limited by the upper bound of its current constraint (i.e. 10 mmol g DW⁻¹
502 h⁻¹) or by light, but instead, it was limited by the amount of carbon skeleton (glutamate) the

503 vegetative cell was able to provide for the incorporation of ammonia. From a stoichiometric
504 point of view, the heterocyst can be forced to produce even more fixed nitrogen from more
505 glutamate, at the expense of vegetative cell growth rate.

506 Growth simulations on thirteen different carbon sources suggested that glucose and sucrose
507 are among the highest yielding substrates, followed by pyruvate, proline, acetate and
508 glutamate. These results were confirmed by growth rate experiments which showed a good
509 overall correlation between the two datasets.

510 Based on these results, all possible combinations of twelve potential exchange metabolites
511 were evaluated in the two-cell model with respect to stoichiometric optimality. Within the
512 simulations, no more than ten exchange reactions were active simultaneously, and the
513 maximum growth rate was achieved by the combination of only seven exchange reactions. A
514 minimum of two exchange metabolites were always required for growth, and the exchange of
515 two metabolites already results in 70% of the maximum growth rate. The best-ranked two
516 metabolite scenario was exchange of ammonia for alanine in the heterocyst. In general, when
517 ammonia was transferred, growth rates were consistently higher by about 3–7% than the
518 growth rates obtained using glutamine as the nitrogen carrier. In case of four reactions
519 inclusion of ammonia increased growth rate by 34–38%, while sucrose was excreted by the
520 heterocyst rather than being consumed. When the heterocyst utilized sucrose as a source of
521 electrons and carbon, however, glutamine, glutamate and 2-oxoglutarate were selected by the
522 model as the best combination for growth, in a good agreement with the literature (Wolk et
523 al., 1976; Thomas et al., 1977; Schilling and Ehrnsperger, 1985; Böhme, 1998; Martin-
524 Figueroa et al., 2000; Picossi et al., 2005; Cumino et al., 2007). Notably, the rate of sucrose
525 transport was closer to reported figures (Nürnberg et al., 2015) when the exchange of
526 glutamine to glutamate was fixed to a 1:1 ratio. The model correctly predicted the importance
527 of sucrose in the vegetative cell-heterocyst system, when glutamine, glutamate and 2-
528 oxoglutarate were also exchanged. However, in many cases higher growth rates were
529 achieved when sucrose was transferred back to the vegetative cell rather than being consumed
530 by the heterocyst, suggesting that stoichiometrically this direction of sucrose exchange is
531 more optimal. In other cases combining the exchange of fructose and sucrose (among other
532 metabolites) the model found a way to ultimately transfer ATP from the heterocyst to the
533 vegetative cell. This transfer utilizing the reverse reaction of fructokinase may be
534 thermodynamically feasible at product concentrations 100-times higher than that of fructose,
535 although there is no evidence that such concentrations occur in a living cell. Nevertheless, it is
536 important to evaluate the consequences of different exchange metabolite combinations, even
537 if the results do not match all experimental observations. In fact, only a model can provide

538 exact answers to stoichiometric optimality, which may be a key in understanding an
539 organism's complex metabolic network.
540 Our model not only provides a comprehensively curated blueprint for the genome-scale
541 metabolic network of *Anabaena* sp. PCC 7120, but also serves as an important computational
542 tool that may allow the design of engineering strategies for the most studied nitrogen-fixing
543 cyanobacterium. Even though *Anabaena* sp. PCC 7120 may primarily be suitable for
544 laboratory research, it is a highly suited first target organism to assess proof-of-principle
545 engineering strategies towards the sustainable production of combined nitrogen (Chaurasia
546 and Apte, 2011) or other important bio-products (Heyer and Krumbein, 1991).
547 In future work, the model would greatly benefit from the inclusion of a more precise biomass
548 equation, specific for *Anabaena* sp. PCC 7120 both under diazotrophic and non-diazotrophic
549 conditions. Such an update of the current biomass equation to reflect the actual elemental
550 composition of the organism's biomass may resolve the discrepancy between the
551 computationally predicted and experimentally observed growth with glutamine.

552 **Materials and Methods**

553 **Metabolic reconstruction of *Anabaena* sp. PCC 7120**

554 A comprehensive protocol for the generation of high quality genome-scale models was
555 followed here (Thiele and Palsson, 2010) to reconstruct the metabolic network of *Anabaena*
556 sp. PCC 7120. Assumptions made during the reconstruction process are collected in
557 Supplemental File S8.

558 The complete genome sequence and gene annotation of *Anabaena* sp. PCC 7120 are available
559 in several databases (Kaneko et al., 2001; Kanehisa et al., 2004; Nakao et al., 2010). The most
560 commonly used annotation was acquired from the curated RefSeq Genome Database of the
561 National Center for Biotechnology Information (NCBI) (Tatusova et al., 2014) and
562 juxtaposed to a recent independent annotation from the J. Craig Venter Institute (JCVI)
563 (Peterson et al., 2001) to pair a meaningful function and a protein product to as many genes as
564 possible. The metabolic function of proteins derived from genomic data was collected from
565 biochemical repositories (Kanehisa et al., 2004; Magrane and Consortium, 2011; Caspi et al.,
566 2012) and primary literature (Supplemental File S3). A systematic, automated algorithm to
567 predict novel gene-protein-reaction (GPR) associations for cyanobacteria was also considered
568 (Krishnakumar et al., 2013) but not used here due to the large number of contradictions to the
569 other sources and experimental data.

570 All the information gathered above was mapped onto general metabolic pathways drawn for
571 the Kyoto Encyclopedia of Genes and Genomes (KEGG) database (Kanehisa et al., 2004) and
572 compared with the data therein. The most recent metabolic reconstruction of the unicellular
573 cyanobacterium *Synechocystis* sp. PCC 6803 (Knoop et al., 2013) was also mapped for
574 comparison and to serve as a template during the identification of critical metabolic functions
575 and gaps. The majority of these gaps were resolved either by finding genes in primary
576 literature or by identifying novel gene/protein candidates based on sequence homology (light
577 and dark pink bands on Figure 8, respectively). Homology-based searches were performed
578 using the BLASTX engine (Altschul et al., 1990) on the NCBI *Anabaena* sp. PCC 7120
579 proteome against gene sequences of reviewed protein entries from the UniProt
580 Knowledgebase (Magrane and Consortium, 2011) to identify best hits. The best hits were
581 verified by BLASTX search against NCBI RefSeq protein database filtered for cyanobacterial
582 entries (Supplemental File S4). A few gaps, otherwise unresolved, were resolved by
583 artificially adding the corresponding metabolic reaction to the model to allow the biosynthesis
584 of key metabolites (e.g. L-methionine and L-asparagine, light green bands on Figure 8) or
585 complete missing steps of close-to-compete pathways (dark green bands). Gaps with over two
586 missing reaction steps were treated differently. In most cases such gaps indicate orphan
587 reactions, and appear in sparsely represented pathways due to misannotation. Lacking any
588 connection to the rest of the network these orphan reactions do not carry metabolic flux in an
589 FBA solution, and were therefore removed from the reconstruction (dark grey bands on
590 Figure 8). Dead-end metabolites not consumed by any reaction in the network were resolved
591 by sink reactions artificially added to the model (yellow bands on Figure 8, also including the
592 biomass equations).

593

594 The equations for each metabolic reaction were adopted either from public databases
595 (Kanehisa et al., 2004; Caspi et al., 2012) or from the *Synechocystis* sp. PCC 6803 model
596 (Knoop et al., 2013). Reaction thermodynamics, in terms of reaction directionality, were
597 either acquired from the MetaCyC database (Caspi et al., 2012) or calculated using
598 eQuilibrator, an online calculator to estimate reactions' Gibbs free energy change (Flamholz
599 et al., 2012). Also, every reaction was evaluated for mass and charge balance using
600 eQuilibrator and adjusted if necessary. Those reactions not found in public resources were set
601 bidirectional. Coenzyme dependencies (NAD⁺, NADP⁺ and quinones) in the KEGG database
602 were adapted for *Anabaena* sp. PCC 7120 wherever primary biochemical evidence was
603 available in the literature or left unchanged (light grey band on Figure 8).

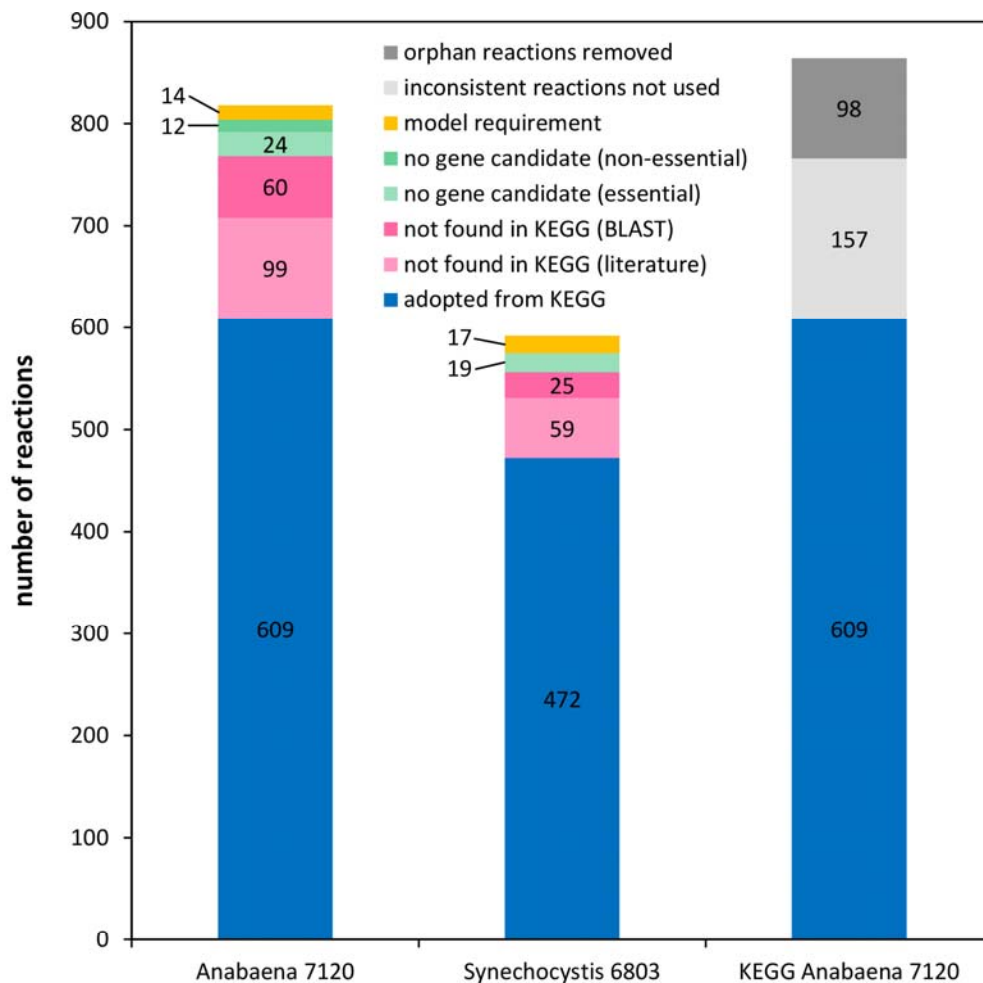


Figure 8. Comparison between *Anabaena* sp. PCC 7120 and *Synechocystis* sp. PCC 6803 (Knoop et al., 2013) stoichiometric models and their improvement over the KEGG database (Kanehisa et al., 2004). Metabolic gaps were resolved by either adapting reactions from literature (light pink bands) or by identifying new gene candidates (dark pink bands). A number of gaps could not be associated with any gene in *Anabaena* sp. PCC 7120 (light and dark green bands). Some reactions in the KEGG database were omitted due to inconsistent coenzyme usage or incomplete reaction formula (light grey band), or due to the lack of connection to the rest of the network (orphan reactions, dark grey band).

604 The stoichiometric model for *Anabaena* sp. PCC 7120 was generated in two formats: as a
 605 single-cell model including photosynthesis and carbon-concentrating reactions for non-
 606 diazotrophic growth in a vegetative cell (Supplemental File S2), and as a two-cell model
 607 setting every reaction to the right super-compartment (either a heterocyst or a vegetative cell)
 608 under diazotrophic conditions (Supplemental File 1). Simulations described in the Results
 609 section, unless otherwise noted, were performed on the two-cell model considering six
 610 intracellular compartments (cytoplasm, cytoplasmic membrane, thylakoid lumen, thylakoid
 611 membrane, carboxysome and periplasmic space) and the external medium (Figure 1).
 612

613 **Stoichiometric simulations and model evaluation**

614 All simulations were run using the COBRA toolbox version 2 with Gurobi Optimizer 5.6.0 as
615 the solver in MATLAB R2103b environment (MATLAB, 2011; Schellenberger et al., 2011;
616 Gurobi Optimization, 2013). All FBA optimizations were calculated using a parameter setting
617 to minimize the taxicab norm. In addition, bicarbonate uptake rate was constrained to an
618 upper bound of $10 \text{ mmol g DW}^{-1} \text{ h}^{-1}$ in phototrophic conditions for both cell types.
619 Simulations with the single-cell model were run on nitrate as the nitrogen source up to 10
620 $\text{mmol g DW}^{-1} \text{ h}^{-1}$, unless otherwise noted. The two-cell model was set to the uptake of
621 molecular nitrogen with an upper limit of $10 \text{ mmol g DW}^{-1} \text{ h}^{-1}$. When comparing single-cell
622 growth on combined nitrogen to the two-cell model under diazotrophic conditions both
623 models were constrained for an equivalent total photon uptake of $10 \text{ mmol g DW}^{-1} \text{ h}^{-1}$. The
624 optimal distribution of the $10 \text{ mmol g DW}^{-1} \text{ h}^{-1}$ photons among the two super-compartments
625 was 7 and 3 $\text{mmol g DW}^{-1} \text{ h}^{-1}$ in the vegetative cell and the heterocyst, respectively. In all
626 other simulations using the two-cell model photon uptake in both super-compartments was
627 constrained to $10 \text{ mmol g DW}^{-1} \text{ h}^{-1}$. For the evaluation of exchange metabolites between the
628 heterocyst and the vegetative cell unconstrained bidirectional diffusion was included to the
629 model for each metabolite.

630 ATP-driven transport reactions have been added to the single-cell model for each carbon and
631 nitrogen source except for molecular nitrogen and ammonia that were exchanged via simple
632 diffusion. In case of mixo- and heterotrophic simulations nitrogen was supplied solely by
633 nitrate, whereas nitrogen sources were compared on bicarbonate in autotrophic conditions. In
634 heterotrophic simulations both photon and bicarbonate uptake rates were set to zero. Under
635 mixotrophic conditions photon and bicarbonate uptake reactions were constrained to 10 mmol
636 $\text{g DW}^{-1} \text{ h}^{-1}$ (millimoles per gram dry cell weight per hour). Both carbon and nitrogen uptake
637 fluxes have been constrained to carry a maximum of $10 \text{ mmol g DW}^{-1} \text{ h}^{-1}$ carbon and nitrogen
638 source, respectively. For example, upper bound of the bicarbonate transport reaction (a single
639 carbon atom) was set to $10 \text{ mmol g DW}^{-1} \text{ h}^{-1}$, whereas glutamine uptake was set to 2 mmol g
640 $\text{DW}^{-1} \text{ h}^{-1}$ (five carbon atoms).

641

642 **Growth rate experiments**

643 Wild-type *Anabaena* sp. strain PCC 7120 was grown in triplicates at 30°C , with continuous
644 illumination from cool white LED lamps at $60 \mu\text{E m}^{-2} \text{ s}^{-1}$, on a rotary shaker at 200 rpm and in
645 sterile 100-ml Erlenmeyer flasks containing 30 ml BG-11 medium (Rippka et al., 1979) until
646 approx. $\text{OD}_{730} = 1$ measured in a 1-cm cuvette. Culture health was evaluated by reading the

647 absorbance spectrum between 300 and 800 nm. The spectra indicated no differences in
648 pigment composition of the biological replicates. The three replicates were then mixed to
649 minimize biological variation. Cells from the mixed wild-type culture were harvested by
650 centrifugation at 3000 g, washed in fresh BG-11, and resuspended to the original volume in
651 fresh BG-11.

652 Each of the BG-11_C media containing one of the organic carbon sources were prepared from
653 the same BG-11 standard medium described elsewhere (Rippka et al., 1979), by replacing
654 bicarbonate for the corresponding organic substrate encapsulating equimolar carbon with 5
655 mM glucose, and filter sterilized. For example, fructose (six carbon atoms per molecule) and
656 glycerol (three carbon atoms per molecule) were set to a final concentration of 5 mM and 10
657 mM, respectively. The washed and resuspended cyanobacterial culture was diluted 10-times
658 in 3 ml of each BG-11_C media and dispensed into 3 wells of untreated 6-well flat-bottom
659 microtiter plates in a pre-randomized fashion. Plates were covered with a sterile lid, wrapped
660 into Parafilm and incubated under the same conditions as the original shake flask cultures.
661 Cyanobacterial growth and health was observed for up to 8 days by optical density
662 measurements in a Tecan M200 Pro plate reader at 730 nm for culture density and 440 nm
663 (absorbance maximum of chlorophyll *a*) for cellular health. The two sets of growth curves
664 acquired at the different wavelengths showed good correlation, and therefore only readings at
665 730 nm were evaluated thereafter. Growth rates were determined for the exponential phase
666 from the growth curves provided on Figure S2 in Supplemental File S10.

667

668 **Supplemental Material**

669

670 **Supplemental File S1.** The reconstructed network of *Anabaena* sp. PCC 7120 under
671 diazotrophic conditions (two-cell model) in a COBRA-compatible SBML format (XML).

672 **Supplemental File S2.** The reconstructed network of *Anabaena* sp. PCC 7120 under non-
673 diazotrophic conditions (single-cell model) in a COBRA-compatible SBML format (XML).

674 **Supplemental File S3.** List of genes, reactions and reconstruction data for both the single-cell
675 and the two-cell model of *Anabaena* sp. PCC 7120 (XLSX).

676 **Supplemental File S4.** List of genes and reactions annotated here for *Anabaena* sp. PCC
677 7120 (XLSX).

678 **Supplemental File S5.** Reactions different in the two super-compartments; orphan reactions
679 and KEGG reaction entries omitted from the working reconstruction (XLSX).

680 **Supplemental File S6.** Interactive metabolic map of the reconstruction in Cytoscape 2.8.3
681 format (CYS).

682 **Supplemental File S7.** Matlab script and map definition files to export COBRA flux
683 distributions and overlay onto the Cytoscape map (ZIP).

684 **Supplemental File S8.** An exhaustive list of assumptions made during the reconstruction
685 process (XLSX).

686 **Supplemental File S9.** Robustness of the model to changes in biomass composition.

687 **Supplemental File S10.** Growth rate comparisons on different carbon and nitrogen sources
688 (PDF).

689

690

Parsed Citations

Adams DG (2000) Symbiotic interactions. In BAWhitton, M Potts, eds, *The Ecology of Cyanobacteria: Their Diversity in Time and Space.* Kluwer Academic Publishers, Dordrecht, pp 523-561

Pubmed: [Author and Title](#)

CrossRef: [Author and Title](#)

Google Scholar: [Author Only](#) [Title Only](#) [Author and Title](#)

Adams DG, Duggan PS (2008) Cyanobacteria-bryophyte symbioses. *Journal of Experimental Botany* 59: 1047-1058

Pubmed: [Author and Title](#)

CrossRef: [Author and Title](#)

Google Scholar: [Author Only](#) [Title Only](#) [Author and Title](#)

Aiello A (1985) Sloth hair: unanswered questions. In GG Montgomery, ed, *The evolution and ecology of armadillos, sloths, and vermilinguas.* Smithsonian Institution Press, Washington, D.C., pp 213-218

Pubmed: [Author and Title](#)

CrossRef: [Author and Title](#)

Google Scholar: [Author Only](#) [Title Only](#) [Author and Title](#)

Albrecht M, Linden H, Sandmann G (1996) Biochemical characterization of purified zeta-carotene desaturase from Anabaena PCC 7120 after expression in Escherichia coli. *Eur J Biochem* 236: 115-120

Pubmed: [Author and Title](#)

CrossRef: [Author and Title](#)

Google Scholar: [Author Only](#) [Title Only](#) [Author and Title](#)

Alexandrova AN, Jorgensen WL (2007) Why Urea Eliminates Ammonia Rather Than Hydrolyzes in Aqueous Solution. *The journal of physical chemistry. B* 111: 720-730

Pubmed: [Author and Title](#)

CrossRef: [Author and Title](#)

Google Scholar: [Author Only](#) [Title Only](#) [Author and Title](#)

Altschul SF, Gish W, Miller W, Myers EW, Lipman DJ (1990) Basic local alignment search tool. *J Mol Biol* 215: 403-410

Pubmed: [Author and Title](#)

CrossRef: [Author and Title](#)

Google Scholar: [Author Only](#) [Title Only](#) [Author and Title](#)

Awai K, Lechno-Yossef S, Wolk CP (2010) Heterocyst Envelope Glycolipids. In H Wada, N Murata, eds, *Lipids in Photosynthesis, Vol 30.* Springer Netherlands, pp 179-202

Pubmed: [Author and Title](#)

CrossRef: [Author and Title](#)

Google Scholar: [Author Only](#) [Title Only](#) [Author and Title](#)

Biswas A (2011) Identification and characterization of enzymes involved in the biosynthesis of different phycobiliproteins in cyanobacteria. University of New Orleans, University of New Orleans Theses and Dissertations

Pubmed: [Author and Title](#)

CrossRef: [Author and Title](#)

Google Scholar: [Author Only](#) [Title Only](#) [Author and Title](#)

Bocchi S, Malgioglio A (2010) Azolla-Anabaena as a Biofertilizer for Rice Paddy Fields in the Po Valley, a Temperate Rice Area in Northern Italy. *International Journal of Agronomy* 2010

Pubmed: [Author and Title](#)

CrossRef: [Author and Title](#)

Google Scholar: [Author Only](#) [Title Only](#) [Author and Title](#)

Bothe H, Nolteernsting U (1975) Pyruvate dehydrogenase complex, pyruvate: Ferredoxin oxidoreductase and lipoic acid content in microorganisms. *Archives of Microbiology* 102: 53-57

Pubmed: [Author and Title](#)

CrossRef: [Author and Title](#)

Google Scholar: [Author Only](#) [Title Only](#) [Author and Title](#)

Böhme H (1998) Regulation of nitrogen fixation in heterocyst-forming cyanobacteria. *Trends in Plant Science* 3: 346-351

Pubmed: [Author and Title](#)

CrossRef: [Author and Title](#)

Google Scholar: [Author Only](#) [Title Only](#) [Author and Title](#)

Caspi R, Altman T, Dreher K, Fulcher CA, Subhraveti P, Keseler IM, Kothari A, Krummenacker M, Latendresse M, Mueller LA, Ong Q, Paley S, Pujar A, Shearer AG, Travers M, Weerasinghe D, Zhang P, Karp PD (2012) The MetaCyc database of metabolic pathways and enzymes and the BioCyc collection of pathway/genome databases. *Nucleic Acids Research* 40: D742-D753

Pubmed: [Author and Title](#)

CrossRef: [Author and Title](#)

Google Scholar: [Author Only](#) [Title Only](#) [Author and Title](#)

Chaurasia AK, Apte SK (2011) Improved Eco-Friendly Recombinant Anabaena sp. Strain PCC7120 with Enhanced Nitrogen Biofertilizer Potential. *Applied and Environmental Microbiology* 77: 395-399

Pubmed: [Author and Title](#)

CrossRef: [Author and Title](#)

Google Scholar: [Author Only](#) [Title Only](#) [Author and Title](#)

Cumino AC, Marcozzi C, Barreiro R, Salerno GL (2007) Carbon cycling in Anabaena sp. PCC 7120. Sucrose synthesis in the heterocysts and possible role in nitrogen fixation. *Plant Physiol* 143: 1385-1397

Pubmed: [Author and Title](#)
CrossRef: [Author and Title](#)
Google Scholar: [Author Only](#) [Title Only](#) [Author and Title](#)

Curatti L, Flores E, Salerno G (2002) Sucrose is involved in the diazotrophic metabolism of the heterocyst-forming cyanobacterium *Anabaena* sp. FEBS Lett 513: 175-178

Pubmed: [Author and Title](#)
CrossRef: [Author and Title](#)
Google Scholar: [Author Only](#) [Title Only](#) [Author and Title](#)

de Macale M, Vlek PG (2004) The role of *Azolla* cover in improving the nitrogen use efficiency of lowland rice. Plant and Soil 263: 311-321

Pubmed: [Author and Title](#)
CrossRef: [Author and Title](#)
Google Scholar: [Author Only](#) [Title Only](#) [Author and Title](#)

Du W, Liang F, Duan Y, Tan X, Lu X (2013) Exploring the photosynthetic production capacity of sucrose by cyanobacteria. Metabolic Engineering 19: 17-25

Pubmed: [Author and Title](#)
CrossRef: [Author and Title](#)
Google Scholar: [Author Only](#) [Title Only](#) [Author and Title](#)

Ehira S (2013) Transcriptional regulation of heterocyst differentiation in *Anabaena* sp. strain PCC 7120. Russian Journal of Plant Physiology 60: 443-452

Pubmed: [Author and Title](#)
CrossRef: [Author and Title](#)
Google Scholar: [Author Only](#) [Title Only](#) [Author and Title](#)

Fay P (1992) Oxygen relations of nitrogen fixation in cyanobacteria. Microbiological Reviews 56: 340-373

Pubmed: [Author and Title](#)
CrossRef: [Author and Title](#)
Google Scholar: [Author Only](#) [Title Only](#) [Author and Title](#)

Feist AM, Henry CS, Reed JL, Krummenacker M, Joyce AR, Karp PD, Broadbelt LJ, Hatzimanikatis V, Palsson B (2007) A genome-scale metabolic reconstruction for *Escherichia coli* K-12 MG1655 that accounts for 1260 ORFs and thermodynamic information. Mol Syst Biol 3: 121

Pubmed: [Author and Title](#)
CrossRef: [Author and Title](#)
Google Scholar: [Author Only](#) [Title Only](#) [Author and Title](#)

Flaherty B, Van Nieuwerburgh F, Head S, Golden J (2011) Directional RNA deep sequencing sheds new light on the transcriptional response of *Anabaena* sp. strain PCC 7120 to combined-nitrogen deprivation. BMC Genomics 12: 332

Pubmed: [Author and Title](#)
CrossRef: [Author and Title](#)
Google Scholar: [Author Only](#) [Title Only](#) [Author and Title](#)

Flamholz A, Noor E, Bar-Even A, Milo R (2012) eQuilibrator—the biochemical thermodynamics calculator. Nucleic Acids Research 40: D770-D775

Pubmed: [Author and Title](#)
CrossRef: [Author and Title](#)
Google Scholar: [Author Only](#) [Title Only](#) [Author and Title](#)

Flores E, Herrero A (2004) Assimilatory Nitrogen Metabolism and Its Regulation. In D Bryant, ed, The Molecular Biology of Cyanobacteria, Vol 1. Springer Netherlands, pp 487-517

Pubmed: [Author and Title](#)
CrossRef: [Author and Title](#)
Google Scholar: [Author Only](#) [Title Only](#) [Author and Title](#)

Flores E, Herrero A (2010) Compartmentalized function through cell differentiation in filamentous cyanobacteria. Nat Rev Micro 8: 39-50

Pubmed: [Author and Title](#)
CrossRef: [Author and Title](#)
Google Scholar: [Author Only](#) [Title Only](#) [Author and Title](#)

Forchhammer K (1999) The PII Protein in *Synechococcus* PCC 7942 Senses and Signals 2-Oxoglutarate Under ATP-Replete Conditions. In G Peschek, W Löffelhardt, G Schmetterer, eds, The Phototrophic Prokaryotes. Springer US, pp 549-553

Pubmed: [Author and Title](#)
CrossRef: [Author and Title](#)
Google Scholar: [Author Only](#) [Title Only](#) [Author and Title](#)

Golden JW, Yoon HS (2003) Heterocyst development in *Anabaena*. Curr Opin Microbiol 6: 557-563

Pubmed: [Author and Title](#)
CrossRef: [Author and Title](#)
Google Scholar: [Author Only](#) [Title Only](#) [Author and Title](#)

Graham JE, Bryant DA (2009) The biosynthetic pathway for myxol-2' fucoside (myxoxanthophyll) in the cyanobacterium *Synechococcus* sp. strain PCC 7002. J Bacteriol 191: 3292-3300

Pubmed: [Author and Title](#)
CrossRef: [Author and Title](#)
Google Scholar: [Author Only](#) [Title Only](#) [Author and Title](#)

- Guarino LA, Cohen SS (1979) Mechanism of toxicity of putrescine in Anacystis nidulans. Proc Natl Acad Sci U S A 76: 3660-3664**
Pubmed: [Author and Title](#)
CrossRef: [Author and Title](#)
Google Scholar: [Author Only](#) [Title Only](#) [Author and Title](#)
- Gurobi Optimization I (2013) Gurobi Optimizer Reference Manual. In,**
Pubmed: [Author and Title](#)
CrossRef: [Author and Title](#)
Google Scholar: [Author Only](#) [Title Only](#) [Author and Title](#)
- Gutzke G, Fischer B, Mendel RR, Schwarz G (2001) Thiocarboxylation of Molybdopterin Synthase Provides Evidence for the Mechanism of Dithiolene Formation in Metal-binding Pterins. Journal of Biological Chemistry 276: 36268-36274**
Pubmed: [Author and Title](#)
CrossRef: [Author and Title](#)
Google Scholar: [Author Only](#) [Title Only](#) [Author and Title](#)
- Harano Y, Suzuki I, Maeda S, Kaneko T, Tabata S, Omata T (1997) Identification and nitrogen regulation of the cyanase gene from the cyanobacteria Synechocystis sp. strain PCC 6803 and Synechococcus sp. strain PCC 7942. Journal of Bacteriology 179: 5744-5750**
Pubmed: [Author and Title](#)
CrossRef: [Author and Title](#)
Google Scholar: [Author Only](#) [Title Only](#) [Author and Title](#)
- Herrero A, Muro-Pastor AM, Flores E (2001) Nitrogen Control in Cyanobacteria. Journal of Bacteriology 183: 411-425**
Pubmed: [Author and Title](#)
CrossRef: [Author and Title](#)
Google Scholar: [Author Only](#) [Title Only](#) [Author and Title](#)
- Heyer H, Krumbein W (1991) Excretion of fermentation products in dark and anaerobically incubated cyanobacteria. Archives of Microbiology 155: 284-287**
Pubmed: [Author and Title](#)
CrossRef: [Author and Title](#)
Google Scholar: [Author Only](#) [Title Only](#) [Author and Title](#)
- Hill DJ (1977) The Role of Anabaena in the Azolla-Anabaena Symbiosis. New Phytologist 78: 611-616**
Pubmed: [Author and Title](#)
CrossRef: [Author and Title](#)
Google Scholar: [Author Only](#) [Title Only](#) [Author and Title](#)
- Hucka M, Finney A, Sauro HM, Bolouri H, Doyle JC, Kitano H, Forum: atrotS, Arkin AP, Bornstein BJ, Bray D, Cornish-Bowden A, Cuellar AA, Dronov S, Gilles ED, Ginkel M, Gor V, Goryanin II, Hedley WJ, Hodgman TC, Hofmeyr J-H, Hunter PJ, Juty NS, Kasberger JL, Kremling A, Kummer U, Le Novère N, Loew LM, Lucio D, Mendes P, Minch E, Mjolsness ED, Nakayama Y, Nelson MR, Nielsen PF, Sakurada T, Schaff JC, Shapiro BE, Shimizu TS, Spence HD, Stelling J, Takahashi K, Tomita M, Wagner J, Wang J (2003) The systems biology markup language (SBML): a medium for representation and exchange of biochemical network models. Bioinformatics 19: 524-531**
Pubmed: [Author and Title](#)
CrossRef: [Author and Title](#)
Google Scholar: [Author Only](#) [Title Only](#) [Author and Title](#)
- Ibarra RU, Edwards JS, Palsson BO (2002) Escherichia coli K-12 undergoes adaptive evolution to achieve in silico predicted optimal growth. Nature 420: 186-189**
Pubmed: [Author and Title](#)
CrossRef: [Author and Title](#)
Google Scholar: [Author Only](#) [Title Only](#) [Author and Title](#)
- Incharoensakdi A, Jantaro S, Raksajit W, Mäenpää P (2010) Polyamines in cyanobacteria: biosynthesis, transport and abiotic stress response. In A Méndez-Vilas, ed, Current Research, Technology and Education Topics in Applied Microbiology and Microbial Biotechnology, Vol Vol 1. Formatex, Spain, pp 23-32**
Pubmed: [Author and Title](#)
CrossRef: [Author and Title](#)
Google Scholar: [Author Only](#) [Title Only](#) [Author and Title](#)
- Jantaro S, Mäenpää P, Mulo P, Incharoensakdi A (2003) Content and biosynthesis of polyamines in salt and osmotically stressed cells of Synechocystis sp. PCC 6803. FEMS Microbiology Letters 228: 129-135**
Pubmed: [Author and Title](#)
CrossRef: [Author and Title](#)
Google Scholar: [Author Only](#) [Title Only](#) [Author and Title](#)
- Kamennaya NA, Chernihovsky M, Post AF (2008) The cyanate utilization capacity of marine unicellular Cyanobacteria. Limnology and Oceanography 53: 2485-2494**
Pubmed: [Author and Title](#)
CrossRef: [Author and Title](#)
Google Scholar: [Author Only](#) [Title Only](#) [Author and Title](#)
- Kamennaya NA, Post AF (2011) Characterization of Cyanate Metabolism in Marine Synechococcus and Prochlorococcus spp. Applied and Environmental Microbiology 77: 291-301**
Pubmed: [Author and Title](#)
CrossRef: [Author and Title](#)
Google Scholar: [Author Only](#) [Title Only](#) [Author and Title](#)

Kanehisa M, Goto S, Kawashima S, Okuno Y, Hattori M (2004) The KEGG resource for deciphering the genome. *Nucleic Acids Research* 32: D277-D280

Pubmed: [Author and Title](#)

CrossRef: [Author and Title](#)

Google Scholar: [Author Only Title Only Author and Title](#)

Kaneko T, Nakamura Y, Wolk CP, Kuritz T, Sasamoto S, Watanabe A, Iriguchi M, Ishikawa A, Kawashima K, Kimura T, Kishida Y, Kohara M, Matsumoto M, Matsuno A, Muraki A, Nakazaki N, Shimpo S, Sugimoto M, Takazawa M, Yamada M, Yasuda M, Tabata S (2001) Complete genomic sequence of the filamentous nitrogen-fixing cyanobacterium *Anabaena* sp. strain PCC 7120. *DNA Res* 8: 205-213; 227-253

Pubmed: [Author and Title](#)

CrossRef: [Author and Title](#)

Google Scholar: [Author Only Title Only Author and Title](#)

Knoop H, Gründel M, Zilliges Y, Lehmann R, Hoffmann S, Lockau W, Steuer R (2013) Flux balance analysis of cyanobacterial metabolism: the metabolic network of *Synechocystis* sp. PCC 6803. *PLoS Comput Biol* 9: e1003081

Pubmed: [Author and Title](#)

CrossRef: [Author and Title](#)

Google Scholar: [Author Only Title Only Author and Title](#)

Krishnakumar S, Durai DA, Wangikar PP, Viswanathan GA (2013) SHARP: genome-scale identification of gene-protein-reaction associations in cyanobacteria. *Photosynth Res*

Pubmed: [Author and Title](#)

CrossRef: [Author and Title](#)

Google Scholar: [Author Only Title Only Author and Title](#)

Kumar K, Mella-Herrera RA, Golden JW (2010) Cyanobacterial heterocysts. *Cold Spring Harb Perspect Biol* 2: a000315

Pubmed: [Author and Title](#)

CrossRef: [Author and Title](#)

Google Scholar: [Author Only Title Only Author and Title](#)

Lechno-Yossef S, Nierzwicki-Bauer S (2002) *Azolla-Anabaena* Symbiosis. In A Rai, B Bergman, U Rasmussen, eds, *Cyanobacteria in Symbiosis*. Springer Netherlands, pp 153-178

Pubmed: [Author and Title](#)

CrossRef: [Author and Title](#)

Google Scholar: [Author Only Title Only Author and Title](#)

Luinenburg I, Coleman JR (1992) Identification, characterization and sequence analysis of the gene encoding phosphoenolpyruvate carboxylase in *Anabaena* sp. PCC 7120. *J Gen Microbiol* 138: 685-691

Pubmed: [Author and Title](#)

CrossRef: [Author and Title](#)

Google Scholar: [Author Only Title Only Author and Title](#)

Luinenburg I, Coleman JR (1993) Expression of *Escherichia coli* phosphoenolpyruvate carboxylase in a cyanobacterium. Functional complementation of *Synechococcus* PCC 7942 ppc. *Plant Physiol* 101: 121-126

Pubmed: [Author and Title](#)

CrossRef: [Author and Title](#)

Google Scholar: [Author Only Title Only Author and Title](#)

Luque I, Forchhammer K (2008) Nitrogen Assimilation and C/N Balance Sensing. In A Herrero, E Flores, eds, *The Cyanobacteria: Molecular Biology, Genomics and Evolution*. Caister Academic Press, pp 336-337

Pubmed: [Author and Title](#)

CrossRef: [Author and Title](#)

Google Scholar: [Author Only Title Only Author and Title](#)

Lynch D, O'Brien J, Welch T, Clarke P, Cuiv PO, Crosa JH, O'Connell M (2001) Genetic organization of the region encoding regulation, biosynthesis, and transport of rhizobactin 1021, a siderophore produced by *Sinorhizobium meliloti*. *J Bacteriol* 183: 2576-2585

Pubmed: [Author and Title](#)

CrossRef: [Author and Title](#)

Google Scholar: [Author Only Title Only Author and Title](#)

Madan AP, Nierzwicki-Bauer SA (1993) In situ detection of transcripts for ribulose-1,5-bisphosphate carboxylase in cyanobacterial heterocysts. *J Bacteriol* 175: 7301-7306

Pubmed: [Author and Title](#)

CrossRef: [Author and Title](#)

Google Scholar: [Author Only Title Only Author and Title](#)

Magrane M, Consortium U (2011) UniProt Knowledgebase: a hub of integrated protein data. *Database* 2011

Pubmed: [Author and Title](#)

CrossRef: [Author and Title](#)

Google Scholar: [Author Only Title Only Author and Title](#)

Malatinszky D, Jones PR (unpublished) Systematic study of biosynthetic genes in the schizokinen operon of *Anabaena* sp. PCC 7120.

Pubmed: [Author and Title](#)

CrossRef: [Author and Title](#)

Google Scholar: [Author Only Title Only Author and Title](#)

Marcozzi C, Cumino AC, Salerno GL (2009) Role of NtcA, a cyanobacterial global nitrogen regulator, in the regulation of sucrose

metabolism gene expression in *Anabaena* sp. PCC 7120. Arch Microbiol 191: 255-263

Pubmed: [Author and Title](#)

CrossRef: [Author and Title](#)

Google Scholar: [Author Only](#) [Title Only](#) [Author and Title](#)

Martin-Figueroa E, Navarro F, Florencio FJ (2000) The GS-GOGAT pathway is not operative in the heterocysts. Cloning and expression of *glsF* gene from the cyanobacterium *Anabaena* sp. PCC 7120. FEBS Lett 476: 282-286

Pubmed: [Author and Title](#)

CrossRef: [Author and Title](#)

Google Scholar: [Author Only](#) [Title Only](#) [Author and Title](#)

MATLAB (2011) MATLAB and Statistics Toolbox Release R2011b. In. The MathWorks Inc., Natick, Massachusetts

Pubmed: [Author and Title](#)

CrossRef: [Author and Title](#)

Google Scholar: [Author Only](#) [Title Only](#) [Author and Title](#)

Meeks JC, Elhai J (2002) Regulation of Cellular Differentiation in Filamentous Cyanobacteria in Free-Living and Plant-Associated Symbiotic Growth States. Microbiology and Molecular Biology Reviews 66: 94-121

Pubmed: [Author and Title](#)

CrossRef: [Author and Title](#)

Google Scholar: [Author Only](#) [Title Only](#) [Author and Title](#)

Mochimaru M, Masukawa H, Maoka T, Mohamed HE, Vermaas WFJ, Takaichi S (2008) Substrate Specificities and Availability of Fucosyltransferase and β -Carotene Hydroxylase for Myxol 2'-Fucoside Synthesis in *Anabaena* sp. Strain PCC 7120 Compared with *Synechocystis* sp. Strain PCC 6803. Journal of Bacteriology 190: 6726-6733

Pubmed: [Author and Title](#)

CrossRef: [Author and Title](#)

Google Scholar: [Author Only](#) [Title Only](#) [Author and Title](#)

Montesinos ML, Herrero A, Flores E (1995) Amino acid transport systems required for diazotrophic growth in the cyanobacterium *Anabaena* sp. strain PCC 7120. Journal of Bacteriology 177: 3150-3157

Pubmed: [Author and Title](#)

CrossRef: [Author and Title](#)

Google Scholar: [Author Only](#) [Title Only](#) [Author and Title](#)

Nakao M, Okamoto S, Kohara M, Fujishiro T, Fujisawa T, Sato S, Tabata S, Kaneko T, Nakamura Y (2010) CyanoBase: the cyanobacteria genome database update 2010. Nucleic Acids Research 38: D379-D381

Pubmed: [Author and Title](#)

CrossRef: [Author and Title](#)

Google Scholar: [Author Only](#) [Title Only](#) [Author and Title](#)

Neilson AH, Larsson T (1980) The utilization of organic nitrogen for growth of algae: physiological aspects. Physiologia Plantarum 48: 542-553

Pubmed: [Author and Title](#)

CrossRef: [Author and Title](#)

Google Scholar: [Author Only](#) [Title Only](#) [Author and Title](#)

Nicolaisen K, Hahn A, Schleiff E (2009) The cell wall in heterocyst formation by *Anabaena* sp. PCC 7120. J Basic Microbiol 49: 5-24

Pubmed: [Author and Title](#)

CrossRef: [Author and Title](#)

Google Scholar: [Author Only](#) [Title Only](#) [Author and Title](#)

Nicolaisen K, Moslavac S, Samborski A, Valdebenito M, Hantke K, Maldener I, Muro-Pastor AM, Flores E, Schleiff E (2008) Alr0397 is an outer membrane transporter for the siderophore schizokinen in *Anabaena* sp. strain PCC 7120. J Bacteriol 190: 7500-7507

Pubmed: [Author and Title](#)

CrossRef: [Author and Title](#)

Google Scholar: [Author Only](#) [Title Only](#) [Author and Title](#)

Nogales J, Gudmundsson S, Knight EM, Palsson BO, Thiele I (2012) Detailing the optimality of photosynthesis in cyanobacteria through systems biology analysis. Proceedings of the National Academy of Sciences

Pubmed: [Author and Title](#)

CrossRef: [Author and Title](#)

Google Scholar: [Author Only](#) [Title Only](#) [Author and Title](#)

Noor E, Bar-Even A, Flamholz A, Reznik E, Liebermeister W, Milo R (2014) Pathway Thermodynamics Highlights Kinetic Obstacles in Central Metabolism. PLoS Comput Biol 10: e1003483

Pubmed: [Author and Title](#)

CrossRef: [Author and Title](#)

Google Scholar: [Author Only](#) [Title Only](#) [Author and Title](#)

Nürnberg DJ, Mariscal V, Bornikoel J, Nieves-Mori3n M, Krauß N, Herrero A, Maldener I, Flores E, Mullineaux CW (2015) Intercellular Diffusion of a Fluorescent Sucrose Analog via the Septal Junctions in a Filamentous Cyanobacterium. mBio 6

Pubmed: [Author and Title](#)

CrossRef: [Author and Title](#)

Google Scholar: [Author Only](#) [Title Only](#) [Author and Title](#)

Owtrim GW, Colman B (1988) Phosphoenolpyruvate carboxylase mediated carbon flow in a cyanobacterium. Biochemistry and Cell Biology 66: 93-99

Pubmed: [Author and Title](#)

CrossRef: [Author and Title](#)

Google Scholar: [Author Only](#) [Title Only](#) [Author and Title](#)

- Pernil R, Herrero A, Flores E (2010) Catabolic Function of Compartmentalized Alanine Dehydrogenase in the Heterocyst-Forming Cyanobacterium *Anabaena* sp. Strain PCC 7120. *Journal of Bacteriology* 192: 5165-5172**
Pubmed: [Author and Title](#)
CrossRef: [Author and Title](#)
Google Scholar: [Author Only](#) [Title Only](#) [Author and Title](#)
- Peterson JD, Umayam LA, Dickinson T, Hickey EK, White O (2001) The Comprehensive Microbial Resource. *Nucleic Acids Res* 29: 123-125**
Pubmed: [Author and Title](#)
CrossRef: [Author and Title](#)
Google Scholar: [Author Only](#) [Title Only](#) [Author and Title](#)
- Picossi S, Montesinos ML, Pernil R, Lichtle C, Herrero A, Flores E (2005) ABC-type neutral amino acid permease N-I is required for optimal diazotrophic growth and is repressed in the heterocysts of *Anabaena* sp. strain PCC 7120. *Mol Microbiol* 57: 1582-1592**
Pubmed: [Author and Title](#)
CrossRef: [Author and Title](#)
Google Scholar: [Author Only](#) [Title Only](#) [Author and Title](#)
- Popa R, Weber PK, Pett-Ridge J, Finzi JA, Fallon SJ, Hutcheon ID, Nealson KH, Capone DG (2007) Carbon and nitrogen fixation and metabolite exchange in and between individual cells of *Anabaena oscillarioides*. *ISME J* 1: 354-360**
Pubmed: [Author and Title](#)
CrossRef: [Author and Title](#)
Google Scholar: [Author Only](#) [Title Only](#) [Author and Title](#)
- Price ND, Papin JA, Schilling CH, Palsson BO (2003) Genome-scale microbial in silico models: the constraints-based approach. *Trends Biotechnol* 21: 162-169**
Pubmed: [Author and Title](#)
CrossRef: [Author and Title](#)
Google Scholar: [Author Only](#) [Title Only](#) [Author and Title](#)
- Razquin P, Fillat MF, Schmitz S, Stricker O, Bohme H, Gomez-Moreno C, Peleato ML (1996) Expression of ferredoxin-NADP+ reductase in heterocysts from *Anabaena* sp. *Biochem J* 316 (Pt 1): 157-160**
Pubmed: [Author and Title](#)
CrossRef: [Author and Title](#)
Google Scholar: [Author Only](#) [Title Only](#) [Author and Title](#)
- Resendis-Antonio O, Reed JL, Encarnación S, Collado-Vides J, Palsson BØ (2007) Metabolic Reconstruction and Modeling of Nitrogen Fixation in *Rhizobium etli*. *PLoS Comput Biol* 3: e192**
Pubmed: [Author and Title](#)
CrossRef: [Author and Title](#)
Google Scholar: [Author Only](#) [Title Only](#) [Author and Title](#)
- Reysenbach AL, Wickham GS, Pace NR (1994) Phylogenetic analysis of the hyperthermophilic pink filament community in Octopus Spring, Yellowstone National Park. *Applied and Environmental Microbiology* 60: 2113-2119**
Pubmed: [Author and Title](#)
CrossRef: [Author and Title](#)
Google Scholar: [Author Only](#) [Title Only](#) [Author and Title](#)
- Rikkinen J, Oksanen I, Lohtander K (2002) Lichen Guilds Share Related Cyanobacterial Symbionts. *Science* 297: 357**
Pubmed: [Author and Title](#)
CrossRef: [Author and Title](#)
Google Scholar: [Author Only](#) [Title Only](#) [Author and Title](#)
- Rippka R, Deruelles J, Waterbury JB, Herdman M, Stanier RY (1979) Generic Assignments, Strain Histories and Properties of Pure Cultures of Cyanobacteria. *Journal of General Microbiology* 111: 1-61**
Pubmed: [Author and Title](#)
CrossRef: [Author and Title](#)
Google Scholar: [Author Only](#) [Title Only](#) [Author and Title](#)
- Ruiz M, Bettache A, Janicki A, Vinella D, Zhang C-C, Latifi A (2010) The *alr2505* (*osiS*) gene from *Anabaena* sp. strain PCC7120 encodes a cysteine desulfurase induced by oxidative stress. *FEBS Journal* 277: 3715-3725**
Pubmed: [Author and Title](#)
CrossRef: [Author and Title](#)
Google Scholar: [Author Only](#) [Title Only](#) [Author and Title](#)
- Saha R, Versept AT, Berla BM, Mueller TJ, Pakrasi HB, Maranas CD (2012) Reconstruction and comparison of the metabolic potential of cyanobacteria *Cyanothece* sp. ATCC 51142 and *Synechocystis* sp. PCC 6803. *PLoS One* 7: e48285**
Pubmed: [Author and Title](#)
CrossRef: [Author and Title](#)
Google Scholar: [Author Only](#) [Title Only](#) [Author and Title](#)
- Schellenberger J, Que R, Fleming RM, Thiele I, Orth JD, Feist AM, Zielinski DC, Bordbar A, Lewis NE, Rahmanian S, Kang J, Hyduke DR, Palsson B (2011) Quantitative prediction of cellular metabolism with constraint-based models: the COBRA Toolbox v2.0. *Nat Protoc* 6: 1290-1307**
Pubmed: [Author and Title](#)
CrossRef: [Author and Title](#)
Google Scholar: [Author Only](#) [Title Only](#) [Author and Title](#)
- Schilling N, Ehrnsperger K (1985) Cellular differentiation of sucrose metabolism in *Anabaena variabilis*. *Z Naturforsch.* 40: 776-779**

Pubmed: [Author and Title](#)
CrossRef: [Author and Title](#)
Google Scholar: [Author Only](#) [Title Only](#) [Author and Title](#)

Schluchter WM, Glazer AN (1997) Characterization of Cyanobacterial Biliverdin Reductase: Conversion of biliverdin to bilirubin is important for normal phycobiliprotein biosynthesis. Journal of Biological Chemistry 272: 13562-13569

Pubmed: [Author and Title](#)
CrossRef: [Author and Title](#)
Google Scholar: [Author Only](#) [Title Only](#) [Author and Title](#)

Serrano A (1992) Purification, characterization and function of dihydroliipoamide dehydrogenase from the cyanobacterium Anabaena sp. strain P.C.C. 7119. Biochemical Journal 288: 823-830

Pubmed: [Author and Title](#)
CrossRef: [Author and Title](#)
Google Scholar: [Author Only](#) [Title Only](#) [Author and Title](#)

Shannon P, Markiel A, Ozier O, Baliga NS, Wang JT, Ramage D, Amin N, Schwikowski B, Ideker T (2003) Cytoscape: A Software Environment for Integrated Models of Biomolecular Interaction Networks. Genome Research 13: 2498-2504

Pubmed: [Author and Title](#)
CrossRef: [Author and Title](#)
Google Scholar: [Author Only](#) [Title Only](#) [Author and Title](#)

Singh RN (1950) Reclamation of /'Usar/' Lands in India through Blue-green Algae. Nature 165: 325-326

Pubmed: [Author and Title](#)
CrossRef: [Author and Title](#)
Google Scholar: [Author Only](#) [Title Only](#) [Author and Title](#)

Singh SP, Montgomery BL (2011) Determining cell shape: adaptive regulation of cyanobacterial cellular differentiation and morphology. Trends Microbiol 19: 278-285

Pubmed: [Author and Title](#)
CrossRef: [Author and Title](#)
Google Scholar: [Author Only](#) [Title Only](#) [Author and Title](#)

Steuer R, Knoop H, Machne R (2012) Modelling cyanobacteria: from metabolism to integrative models of phototrophic growth. J Exp Bot 63: 2259-2274

Pubmed: [Author and Title](#)
CrossRef: [Author and Title](#)
Google Scholar: [Author Only](#) [Title Only](#) [Author and Title](#)

Stewart WD, Rowell P, Rai AN (1983) Cyanobacteria-eukaryotic plant symbioses. Ann Microbiol (Paris) 134b: 205-228

Pubmed: [Author and Title](#)
CrossRef: [Author and Title](#)
Google Scholar: [Author Only](#) [Title Only](#) [Author and Title](#)

Takaichi S, Mochimaru M (2007) Carotenoids and carotenogenesis in cyanobacteria: unique ketocarotenoids and carotenoid glycosides. Cell Mol Life Sci 64: 2607-2619

Pubmed: [Author and Title](#)
CrossRef: [Author and Title](#)
Google Scholar: [Author Only](#) [Title Only](#) [Author and Title](#)

Takaichi S, Mochimaru M, Maoka T, Katoh H (2005) Myxol and 4-ketomyxol 2'-fucosides, not rhamnosides, from Anabaena sp. PCC 7120 and Nostoc punctiforme PCC 73102, and proposal for the biosynthetic pathway of carotenoids. Plant Cell Physiol 46: 497-504

Pubmed: [Author and Title](#)
CrossRef: [Author and Title](#)
Google Scholar: [Author Only](#) [Title Only](#) [Author and Title](#)

Tatusova T, Ciufu S, Fedorov B, O'Neill K, Tolstoy I (2014) RefSeq microbial genomes database: new representation and annotation strategy. Nucleic Acids Res 42: D553-559

Pubmed: [Author and Title](#)
CrossRef: [Author and Title](#)
Google Scholar: [Author Only](#) [Title Only](#) [Author and Title](#)

Thiele I, Palsson B (2010) A protocol for generating a high-quality genome-scale metabolic reconstruction. Nat Protoc 5: 93-121

Pubmed: [Author and Title](#)
CrossRef: [Author and Title](#)
Google Scholar: [Author Only](#) [Title Only](#) [Author and Title](#)

Thomas J, Meeks JC, Wolk CP, Shaffer PW, Austin SM (1977) Formation of glutamine from [13n]ammonia, [13n]dinitrogen, and [14C]glutamate by heterocysts isolated from Anabaena cylindrica. J Bacteriol 129: 1545-1555

Pubmed: [Author and Title](#)
CrossRef: [Author and Title](#)
Google Scholar: [Author Only](#) [Title Only](#) [Author and Title](#)

Valladares A, Herrero A, Pils D, Schmetterer G, Flores E (2003) Cytochrome c oxidase genes required for nitrogenase activity and diazotrophic growth in Anabaena sp. PCC 7120. Molecular Microbiology 47: 1239-1249

Pubmed: [Author and Title](#)
CrossRef: [Author and Title](#)
Google Scholar: [Author Only](#) [Title Only](#) [Author and Title](#)

Valladares A, Maldener I, Muro-Pastor AM, Flores E, Herrero A (2007) Heterocyst Development and Diazotrophic Metabolism in Terminal Respiratory Oxidase Mutants of the Cyanobacterium Anabaena sp. Strain PCC 7120. Journal of Bacteriology 189: 4425-

4430

Pubmed: [Author and Title](#)
CrossRef: [Author and Title](#)
Google Scholar: [Author Only](#) [Title Only](#) [Author and Title](#)

van Bodegom P (2007) Microbial Maintenance: A Critical Review on Its Quantification. Microbial Ecology 53: 513-523

Pubmed: [Author and Title](#)
CrossRef: [Author and Title](#)
Google Scholar: [Author Only](#) [Title Only](#) [Author and Title](#)

Vu TT, Stolyar SM, Pinchuk GE, Hill EA, Kucek LA, Brown RN, Lipton MS, Osterman A, Fredrickson JK, Konopka AE, Beliaev AS, Reed JL (2012) Genome-scale modeling of light-driven reductant partitioning and carbon fluxes in diazotrophic unicellular cyanobacterium *Cyanothece* sp. ATCC 51142. PLoS Comput Biol 8: e1002460

Pubmed: [Author and Title](#)
CrossRef: [Author and Title](#)
Google Scholar: [Author Only](#) [Title Only](#) [Author and Title](#)

Wagner G (1997) Azolla: A review of its biology and utilization. The Botanical Review 63: 1-26

Pubmed: [Author and Title](#)
CrossRef: [Author and Title](#)
Google Scholar: [Author Only](#) [Title Only](#) [Author and Title](#)

Wolk CP, Ernst A, Elhai J (2004) Heterocyst Metabolism and Development. In D Bryant, ed, The Molecular Biology of Cyanobacteria, Vol 1. Springer Netherlands, pp 769-823

Pubmed: [Author and Title](#)
CrossRef: [Author and Title](#)
Google Scholar: [Author Only](#) [Title Only](#) [Author and Title](#)

Wolk CP, Thomas J, Shaffer PW, Austin SM, Galonsky A (1976) Pathway of nitrogen metabolism after fixation of ¹³N-labeled nitrogen gas by the cyanobacterium, *Anabaena cylindrica*. J Biol Chem 251: 5027-5034

Pubmed: [Author and Title](#)
CrossRef: [Author and Title](#)
Google Scholar: [Author Only](#) [Title Only](#) [Author and Title](#)